Department of Precision and Microsystems Engineering

Dynamics of microfluidic cantilevers in a photothermal AFM

Stijn Paardekooper

Report no : 2021.044
Coach : Dr. Gerard J. Verbiest & Dr. Murali K. Ghatkesar
Professor : Dr. Gerard J. Verbiest & Dr. Murali K. Ghatkesar
Specialisation : Dynamics of Micro and Nanosystems
Type of report : MSc Thesis
Date : July 7, 2021

Dynamics of microfluidic cantilevers in a photothermal AFM

by

Stijn Paardekooper

For the degree of Master of Science in Mechanical Engineering
at Delft University of Technology,
submitted on July 7, 2021

Student number: 4982266
Thesis committee:
Dr. Gerard J. Verbiest
Dr. Murali K. Ghatkesar
Dr. Farbod Alijani

TU Delft
July 7, 2021


TU Delft
Delft
University of
Technology

Acknowledgements

It would have been impossible to complete this project without the help from my supervisors, fellow students, friends and family.
Firstly, I would like to thank my supervisors Gerard and Murali, your combined expertise in optics, acoustics, MEMS and microfluidics was extremely helpful during my research. On top of this you helped me stay motivated whenever things weren't going my way. I'm very grateful for the amount of time and effort you've put into guiding me.
I would also like to thank postdocs and PhD students: Ruben, Martin Robin, Tomas and Martin Lee for helping me around the lab, brainstorming with me or collaborating with me on my project. Your efforts are much appreciated.
Finally I would like to thank my parents, friends and family for their sympathetic ear and motivation throughout the past year.

Stijn Paardekooper
July 7, 2021

Contents

Abstract

Any resonance based sensing method such as AFM or mass sensing using microfluidic cantilevers require high frequency stability. For mass measurement, a stable frequency allows for a lower mass resolution. One of the most commonly used methods to actuate these resonators is using piezoacoustics. A major downside of this method is the presence of spurious resonances, which corrugate the frequency response and can potentially degrade mass sensitivity. One way get rid of these spurious peaks is by actuating photothermally (using laser light). This thesis is focused around designing and building a photothermal AFM to explore this. Additionally, some experiments are performed comparing piezoacoustic actuation to photothermal actuation in terms of the aforementioned frequency stability and spurious peaks.

1 Introduction

In 2012, Chaste et al. reached a mass resolution of 1.7 yoctogram (1.7×10^{-24}g) using a nanomechanical resonator in vacuum [1]. Suspended Microchannel Resonators (SMR) use a similar working principle but allow samples to be submerged in the liquid inside of the cantilever. Accurate, highly sensitive mass measurement has proven its significance in a wide spectrum of research over the past years. From studying cell growth [2] to response to drugs [3] [4]. Besides detecting changes in mass, microfluidic cantilevers have also been used to characterize polymers by detecting their transition temperatures via changes in stiffness [5]. The focus of this study concerns the excitation method. The current microfluidic cantilevers are mainly excited using piezoacoustics, which often show corrugated frequency responses. This problem also occurs in Atomic Force Microscopy (AFM), where solid, rectangular cantilevers are used. For these cantilevers, exciting with a laser (photothermally) instead of piezoacoustically resulted in a much cleaner response. The question remains if this method of exciting also works with microfluidic cantilevers.
As mentioned, photothermal excitation is not a new principle. It has been applied numerous times within AFMs to combat spurious resonances [6–11]. However, no research has been done on exciting microfluidic cantilevers using photothermal excitation. The vastly more complicated geometry, as well as the fluid flowing inside of it makes the adoption of this excitation scheme less trivial. The extra thermal energy introduced into the system may degrade its performance. In addition, there is currently no photothermal AFM present at the mechanical engineering faculty.

The goal of this thesis project is to design and build a photothermal AFM for actuating microfluidic cantilevers and to study the differences in frequency stability.

The remainder of this introduction section will include basic working principles of resonant based sensors, excitation and measurement methods. The problem of spurious resonances is also introduced, and photothermal excitation as a means to get rid of them. Then different kinds of noise are introduced, followed by an overview of the starting point of the experimental setup. Finally, Allan deviation is introduced as a unit to quantify frequency stability along with the research questions of this thesis.
After this introductory section, the building process is described in the methods section. This section touches upon the numerous issues encountered while building and how they were solved, finishing with an overview of the final/current setup.
After the methods section, a paper on this study is included. The results of this study are described concisely (along with a similar introductory and methods section), after which they are discussed and conclusions are drawn.
Finally, some overall conclusions are drawn, followed by recommendations, future work and a self-reflection.

1.1 AFM and SMR working principle

An Atomic Force Microscope (AFM) creates an image of a sample by "feeling" the sample in a similar manner to sliding your finger over a surface to get a sense of its topography. This is unlike the well

known optical microscopes, which magnify a sample using lenses. At the heart of every AFM, there is a small cantilever with a sharp tip at the end. This tip senses the provided sample by either touching the sample or vibrating very close to the sample. The interaction between the tip and the sample causes the cantilever to bend (or change frequency in the vibrating case). This change is counteracted using a feedback loop, which changes the tip-sample distance to keep the frequency constant. The feedback signal is translated to a height on that point. By sweeping the surface, the AFM is able to create an image of the complete sample.

Microfluidic cantilevers, or Suspended Microchannel Resonator (SMR) are another commonly used resonant sensor. The working principle of SMRs are similar to the AFM, but instead of measuring the topography of a sample, the cantilevers are used to measure other quantities such as: mass, density and viscosity [12–14]. These measurement techniques make use of the mass dependency of the cantilevers resonance frequency by vibrating the cantilever, and measuring changes in their resonance frequency due to changes in mass. Conventionally, this increase in mass is achieved by letting particles land or bind on the surface of the cantilever, which result in a decrease of the resonance frequency. While this technique works well in a gaseous environment, in liquid the large viscous drag and increase effective mass imposed by the liquid surrounding the cantilever causes a large increase in the damping [15–17]. The amount of damping is hereafter expressed in Q-factor: The ratio between energy stored and energy loss (the higher the Q-factor, the lower the damping).

The SMR effectively solves this problem by, instead of submerging the cantilever in liquid, the liquid is put into the cantilever. Which makes it possible to measure masses which need to be submerged in liquid, such as living cells [18–20] or biological molecules [21]. The cantilevers used for this are typically U-shaped and hollow (figure 2).

Because the cantilever can be accurately modeled using the Bernoulli-Euler beam model, we can calculate its resonance frequency f_0 from the following equation:

$$f_0 = \frac{1}{2\pi}\sqrt{\frac{k}{m_{eff}}} \tag{1}$$

With m_{eff} and k being the effective mass and stiffness respectively. When a mass Δm is flowing through the channel, the resonance frequency shifts [21]:

$$f_0 = \frac{1}{2\pi}\sqrt{\frac{k}{m_{eff} + \alpha\Delta m}} \tag{2}$$

With α being a numerical constant that depends on the geometric localization of the added mass. When the mass reaches the tip of the cantilever, $\alpha \approx 1$.

Figure 1 shows a schematic representation of the shift in resonance frequency as a particle moves through the cantilever.

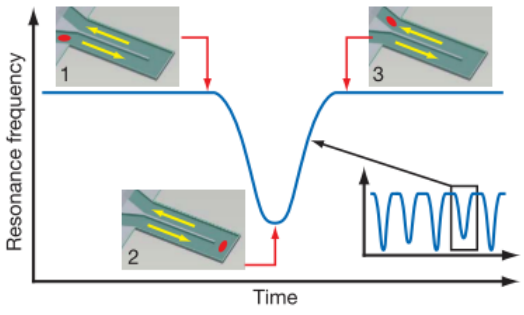

Figure 1: Schematic representation of particle detection [21]

(a) (b)

Figure 2: (a) U-shaped hollow cantilever and its (b) cross-section [22]

A common figure of merit for SMRs is the mass responsivity $\Re$, which is defined as the change in frequency due to a change in mass [23]:

$$\Re = \frac{\partial f_0}{\partial m} \approx -\frac{1}{2}\frac{f_r}{m_{eff}} \tag{3}$$

As can be seen from equation 3 and equation 1, mass responsivity can be increased by reducing the mass of the cantilever and/or increasing its stiffness. The desire for a low mass explains why typical cantilevers are fabricated at the micro or even nanoscale. Another important figure of merit is the mass resolution δm, which is the minimum detectable mass. The mass resolution is defined as the ratio between frequency noise and responsivity [24, 25]:

$$\delta m \approx \frac{\delta f}{\Re} = -2m\frac{\delta f}{f_r} \approx -2m_{eff}\frac{1}{Q}\frac{\text{Noise}}{\text{Signal}} \tag{4}$$

In order to achieve a low mass resolution, it's important to have a low effective mass, as well as high Q-factor and a high signal-to-noise ratio (which will be discussed in a later section).

1.2 Detection methods

The frequency detection of the cantilever is an important step in the measurement scheme which makes its discussion essential for this literature study. The most commonly used detection methods are discussed in this section: Laser Doppler vibrometry, the optical lever method and self sensing methods.

1.2.1 Laser Doppler vibrometry

Laser Doppler vibrometry (LDV) determines the vibration of a surface by measuring the Doppler shift of a reflected laser beam. A beam splitter splits the laser into a reference beam and a test beam. The reference beam hits the photodetector immediately. The test beam is typically frequency shifted before hitting the specified target, after which it reflects and gets redirected to the photodetector. The optical detector detects the beat frequency between the two beams which can be demodulated to derive the frequency shift due to the Doppler effect, which is a function of the targets velocity.

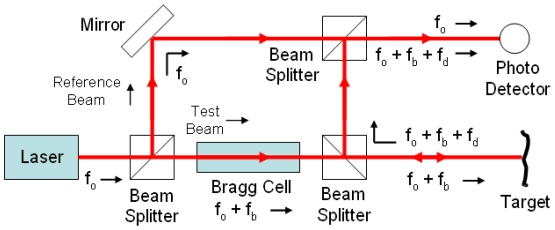

Figure 3: Schematic of a laser Doppler vibrometer [26]

LDV commonly possesses the ability to scan a surface by measuring a grid of points. This enables the user to extract information about the different mode shapes. This is one of the key advantages of using this technique for measuring MEMS, along with not having to modify the sample. An important disadvantage is the presence of a laser which might cause temperature side effects (this will be discussed further in section 1.5.4) as well as the high price range of these devices.

1.2.2 Optical lever method

The optical lever method, or sometimes called optical beam deflection method, works via a laser which is focused onto the cantilever and reflected to an array of photodiodes. As the cantilever bends, the angle of reflection changes, which means the reflected beam changes its position on the array of photodiodes. The voltage of these photodiodes can be used to determine the deflection of the cantilever.

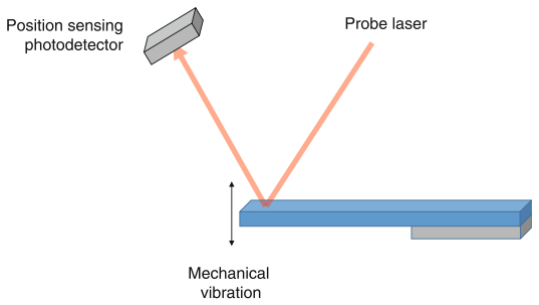

Figure 4: Schematic of the optical lever method [27]

This method remains popular since its invention in 1988 due to its simplicity, ease-of-use and sub-nanometer sensitivity [28], [29]. A key disadvantage however is the need for a reflective coating in order to keep the signal to noise ratio high. The laser is aimed at the tip of the cantilever in order to measure the largest displacement. This position is however considered least ideal in terms of temperature management; due to the small cross-section, conduction is limited and elevated steady-state temperatures can cause a frequency drift (this will be further discussed in section 1.5.4).

1.2.3 Self-sensing methods

The self-sensing methods that are discussed in this section are the piezoresistive, piezoelectic and the capacitive method.

Piezoresistive method

The piezoresistive method works by placing p-doped resistors at high stress regions of the cantilever. The piezoresistive effect causes the resistance to change due to the mechanical stress. This change in resistance can be measured and used to calculate the deflection of the cantilever. An advantage of this method is the compact nature of the setup which allows for miniaturization (e.g for lab-on-chip devices). Disadvantages are the need to alter the cantilevers [28].

Piezoelectric method

Similar to the piezoresistive method, the piezoelectric method makes use of the piezoelectric effect by placing a piezoelectric film on the cantilever surface. The piezoelectric effect enables the film to be used for both actuation and detection and is also suitable for lab-on-chip devices. An additional advantage is the low heat generation due to the low current. One of the biggest drawbacks of this method is the added mass of the piezoelectric film, which lowers the responsitivity [27].

Capacitive detection

In capacitive detection, the capacitance is measured between two electrodes, one being the cantilever and the other one placed close to the cantilever. Displacement of the cantilever causes the distance between

the electrodes to shrink, which results in a change in capacitance. A well known disadvantage is the decrease in sensitivity when miniaturizing the device due to the proportionality between capacitance and electron area. Advantages are high sensitivity and overal simplicity [24].

1.3 Excitation methods

Since the invention of the AFM and SMR, a lot of effort has been made to come up with better ways to actuate the cantilever. The most frequently used excitation methods, each with their own advantages and disadvantages, are discussed in this section. Except for photothermal excitation, which, due to its relevance to this study, is separately discussed in section 1.5.

1.3.1 Piezoacoustic excitation

Because of its ease of implementation, ease-of-use and low cost, piezoacoustic excitation is the most used excitation method in AFMs [28]. Its working principle is simple: a piezoelectric actuator is placed somewhere on the setup (usually the chip-holder). The cantilever is excited by vibrating the actuator. However, not only the cantilever is excited, but also the chip and chip holder, along with other parts in close proximity of the actuator. This causes spurious resonances, which are discussed more thoroughly in section 1.4.

1.3.2 Magnetic excitation

Magnetic excitation works by creating a changing magnetic field around the (magnetic) cantilever, which causes it to vibrate. In order to achieve this, the cantilever must first be modified by either gluing a small magnet onto the cantilever or sputtering the cantilever with a magnetic material. The former causes a mass increase due to the weight of the epoxy and the magnet, which is why the latter is used more commonly. Magnetic excitation provides very clean results, even in liquid [30]. However, major drawbacks such as contamination by magnetic ions and poor repetitive production makes magnetic excitation one of the least used methods of excitation [28].

1.3.3 Electrostatic excitation

Electrostatic excitation is similar to capacitive detection and is considered the most widespread excitation method for SMRs [24]. In electrostatic excitation, the cantilever functions as an electrode, with another electrode in close proximity of the cantilever. Applying a voltage between these electrodes causes an electrostatic force which is used to excite the cantilever [31]. The fast response, low power consumption and ease-of-use makes this method of excitation favourable for a lot of applications. Some drawbacks are its nonlinear response, the need for a high-compliant cantilever due to the weak interaction forces [28], the weak performance at the nanoscale due to the scaling mentioned previously and the high sensitivity to electrostatics [32] when not properly shielded, external fields may influence the measurement.

1.4 Spurious resonances

A piezoactuator is unable to focus its energy on vibrating *just* the cantilever. As a result, the chip, the holder and other objects surrounding the cantilever vibrate. These spurious resonances, which are commonly called the "forest-of-peaks" are measured which causes a polluted frequency response, as seen for example in figure 5a (blue line). This forest-of-peaks also originates from the piezo-shaker [35] and is most well known in liquid environments. This is due to the low Q-factor of the cantilever in liquids (typically between 1 and 5). Even though these peaks are less apparent in air and vacuum, it has been recognized that their effects are important at low temperatures and high vacuum [34], which is common practice in order to lower the noise floor and increase mass resolution. This is clearly seen in figure 5b, at

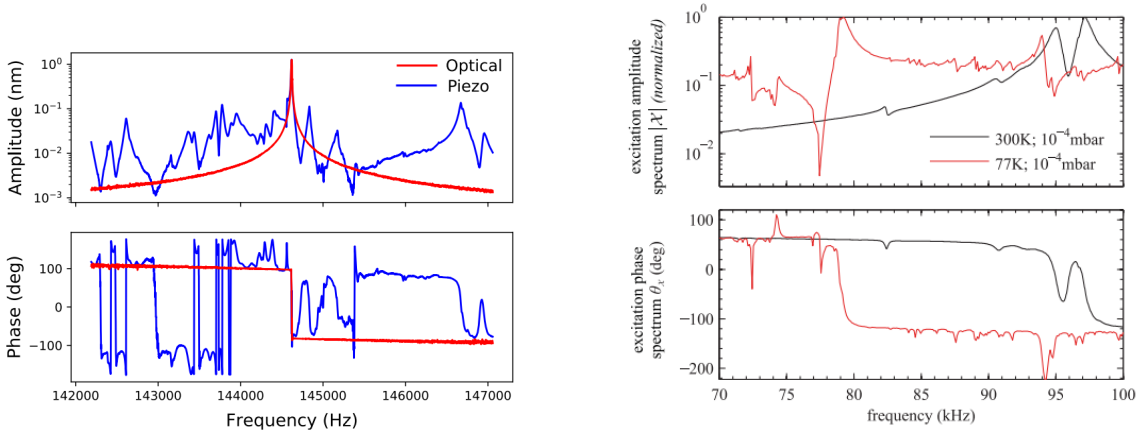

(a) (b)

Figure 5: (a) Frequency response of the cantilever amplitude around resonance in liquid [33] (b) Transfer function of the piezoacoustic excitation system at two different temperatures in vacuum [34]

lower temperature and pressure, the piezo shaker has an extremely non-flat response. Studies that have compared photothermal and piezo excitation in AFM [33, 36] all recommended photothermal excitation over piezoacoustics. Labuda et al. [36] concludes that recovering the frequency shift in a piezoacoustic excited system requires a numerical approach. A simulation shows that a slight shift in resonance causes an apparent oscillator damping signal. They also conclude that the phase and amplitude signal of a photothermally excited signal remain lineair and stable across a wide bandwidth. Even though this study was performed in a liquid environment, Miyahara et al. [33] found similar results in air. Besides the published sources mentioned above, a fellow master student at the TU Delft is determining the mass of nano-plastics by using an SMR. The frequency response of his cantilever can be seen in figure 6. The frequency response is very polluted with spurious resonances, which we hope to resolve using photothermal excitation.

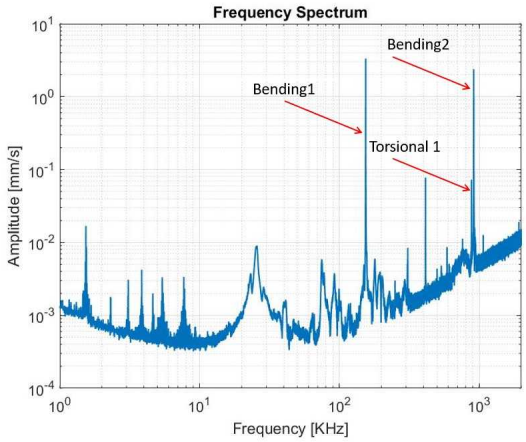

Figure 6: Frequency response of a fellow student at the TU Delft

1.5 Photothermal excitation

In photothermal excitation, a modulated laser is focused on the resonator which locally heats up due to the photothermal effect. Periodic expansion and contraction due to a heat induced stress gradient in

the cantilever causes it to vibrate. While exciting AFM cantilevers photothermally has been extensively studied [10, 36–39], a knowledge gap becomes apparent when looking for papers on photothermally exciting SMRs. So far, only R. A. Barton et al. [40] has looked into this. However, this paper describes a clamped-clamped resonator on a scale much smaller than a typical singly clamped SMR.
Because of the similarities between AFM and SMRs, we can learn a lot from previous studies on photothermal AFMs and make predictions on how it will perform on an SMR.

1.5.1 Coated cantilevers

The amplitude of deflection due to the photothermal effect can be greatly enhanced by coating the cantilever. This is due to the bimaterial effect: A difference between the thermal expansion coefficients of the two materials causes bending of the cantilever. The magnitude of this effect will further be explained in the next section. Other artifacts of a coated cantilever include:

- Change of resonance frequency due to change in stiffness, mass and thickness [41–43].
- Change in reflectivity, which changes the amount of energy absorbed by the incident light. This also changes the amount of light reflected by the measurement laser, which directly affects the signal-to-noise ratio [44].
- Change in resonance frequency due to the thermal mismatch between the cantilever material and the coating material [42].

1.5.2 Driving force

For uncoated cantilevers, the primary driving force is due to the momentum transfer between the photons and the cantilever, and can be expressed as [45]:

$$F = (1 + r - t)\frac{I_{\text{in}}}{c}\cos\alpha \tag{5}$$

Where r and t are the reflectance and transmittance coefficient respectively, c is the speed of light, I_{in} the input intensity and α the angle of incidence of the light. Marti et al. [45] also investigated the bending effect due to the temperature gradient caused by uneven heating of the cantilever over the z axis. They found a negligible equivalent force of 0.064fN.
The driving force induced by the laser is, in case of a coated cantilever, primarily caused by the difference in thermal expansion coefficients of the two materials [39]:

$$F_{drive}(x \mid \nu) = c_{th}(\nu)\frac{\partial^2}{\partial x^2}T(x,\nu)\delta\left(\nu - \nu_{ex}\right)e^{i2\pi\nu t_0} \tag{6}$$

Where $T(x)$ is the spatial temperature profile produced on the cantilever, ν and ν_{ex} are the vibrational frequency and excitation frequency respectively, x_0 is the position of the excitation laser relative to the base, t_0 is the delay between the laser signal and the cantilever deflection and c_{th} is the bending moment coefficient:

$$c_{th} = W\left[\alpha_1 E_1 d_1\left(\frac{d_1}{2} - z_0\right) - \alpha_2 E_2 d_2\left(z_0 - \frac{d_2}{2}\right)\right] \tag{7}$$

Where W is the width of the cantilever, α is the thermal expansion coefficient, E is the Youngs modulus, d the thickness and z_0 is the distance between the neutral axis and the bimaterial interface [10].
Even though the above equations are derived for a rectangular cantilever, one can expect an SMR to behave in a similar manner. This makes it useful for a future theoretical model or simply gaining an intuition for the laser induced driving force and its dependent variables.
The driving force being dependent on the distance x_0 suggests that there is an optimal spot for driving the resonator, which is discussed in the following subsection.

1.5.3 Driving point

As mentioned in the previous section, Pini et al. [10], as well as Ramos et al. [39] investigated the photothermal driving force, which turns out is a function of the excitation position. Pini reports that the photothermal effect is proportional to the second spatial derivative of the normal modes, which means the optimal driving point is optimal where the curvature is at a maximum. Therefore, for exciting the first mode, close to the base is optimal. Whereas for the second mode, more towards the middle is optimal.
One should also take into account the heating effects of the laser. Which, in vacuum, can increase dramatically when moving closer to the end of the cantilever as described by Sandoval et al. [44] (figure 7).

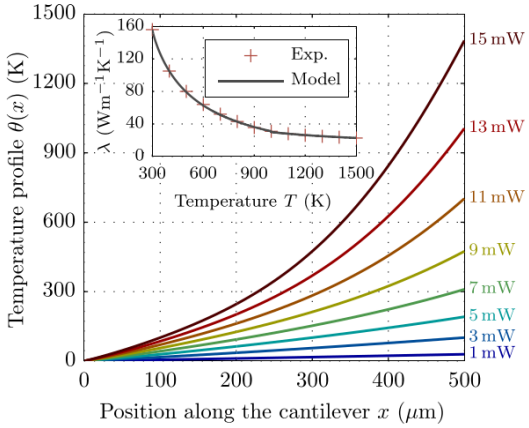

Figure 7: Temperature profile vs. Position relative to the base of a 500μm rectangular cantilever [44]

Similar conclusions are also drawn by Ratcliff et al. [7], who found the optimal laser position to be 1-2.5 times the decay length. Intuitively, this can be substantiated by realising that a strong cantilever bending is optimal at the base of the beam because it magnifies its displacement at the end. Bircher et al. [46] found the optimal position to be close to the base for all modes, probably due to the thicker region at the base acting as a heat sink. The heat sink allows for higher local peak-to-peak temperature variations which are transduced into higher amplitudes.

1.5.4 Temperature side-effects

Many studies have observed frequency shifts of microresonators due to heat. There are numerous thermo-elastic coupling effects at play here, which are discussed in this section.
The Young's modulus E is temperature dependent. In the case of silicon, this dependency (α_E) is negative. This means a decrease in stiffness with increasing temperature [42, 44, 47]:

$$\alpha_E = \frac{1}{E}\frac{\mathrm{d}E}{\mathrm{d}T} \approx -64 \cdot 10^{-6}\mathrm{K}^{-1} \tag{8}$$

A decrease in stiffness causes a decrease in resonance frequency (equation 1). However, experiments conducted by Sandoval et al. [44] show results contradicting this theory. Namely a mode dependency on the frequency shift, and even a frequency increase for a larger cantilever in air with increasing temperature. Sandoval derives a theoretical model to show the mode dependency of the frequency shift in cantilevers due to a temperature difference:

$$\frac{\delta\omega_n}{\omega_n} = \frac{1}{2}\alpha_E \frac{1}{\alpha_n^4}\int_0^1 \mathrm{d}x\theta(x)\left(\frac{\mathrm{d}^2\phi_n^0}{\mathrm{d}x^2}\right)^2 \tag{9}$$

Here we can clearly recognize the frequency shift being dependent on, not only the change in Young's modulus due to temperature (α_E), but also by the square of the local curvature of the specific mode shape (on a normalized length scale x from the base of the cantilever, with arbitrary temperature profile $\theta(x)$). This equation does not take into account the presence of the air surrounding the cantilever.
The air around the cantilever also influences its resonance. Not only the cantilever increases in temperature, but also the air around it. Causing it to increase in viscosity and decrease in density. A certain volume of the air around the cantilever can be seen as part of its effective mass (m_{eff}) [15]. A decrease in density decreases this effective mass, which in turn increases its resonance frequency (equation 1). This phenomenon is strongly dependent on the cantilever geometry.
Another, less significant effect, is the expansion of the geometry due to heat. This effect is often neglected since it's about an order of magnitude smaller than the change in Young's modulus [44].
Sondoval et al. also estimated the maximum temperatures in vacuum. Figure 7 shows the temperature dependence on position from the base, and figure 8 shows the maximum temperature (at the tip) dependent on the light intensity. From both figures, it can be concluded that temperatures in vacuum can reach temperatures which could ultimately melt the silicon cantilever. The temperature increase remains relatively low when staying close to the base.

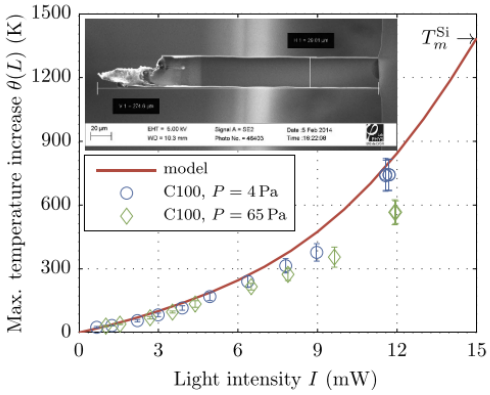

Figure 8: Maximum temperature increase vs. Light intensity [44]

The effects mentioned above have also been found to be caused by the measurement laser [46, 48, 49].

1.6 Noise sources

The scientific community continuously works towards smaller mass resolutions, and as cantilevers get smaller and lighter, the influence of noise grows. This is why a good understanding of the different noise sources is indispensable when studying microresonators. Different noise sources will be discussed in this section, with a primary focus on temperature dependence, since a rise in temperature is inevitable when switching to photothermal excitation.

1.6.1 Thermomechanical noise

When the SMR is in equilibrium and no drive signal is applied, it will still exhibit tiny movements. This is due to thermomechanical noise. The equipartition theorem states that, for each degree of freedom, cantilever movement z due to this noise given by:

$$\langle z^2 \rangle = \frac{k_B T}{k} \tag{10}$$

Where $\langle z^2 \rangle$ is the mean square displacement of the SMR, k_B is the Boltzmann constant, T temperature and k the stiffness of the cantilever. Using this equation, combined with the transfer function of

a one-dimensional harmonic oscillator, one can construct an expression for the relative uncertainty in determining the resonance frequency shift [32]:

$$\frac{\sqrt{\left\langle \left(\widehat{\omega_0} - \omega_0\right)^2 \right\rangle}}{\omega_0} = \sqrt{\frac{k_B T k}{\tau \omega_0}} \frac{1}{Q^{3/2} F_0} \tag{11}$$

With ω_0 being the resonance frequency and F_0 the driving force amplitude. τ is the time constant of the lock-in detection, which indicates how fast the frequency tracking hardware can respond to changes in the resonant frequency. The lock-in setup is described in more detail in the next section. It can easily be seen that the uncertainty increases with increasing temperature and decreases with increasing Q-factor and driving amplitude. The latter is obviously limited by the mechanical properties of the SMR. These properties result in some interesting tradeoffs, namely: An increase in Q-factor is most effectively done by measuring in vacuum, however this leads to an increase in temperature due to limited heat dissipation via convection. An increase in temperature will however most likely result in the increase of the drive amplitude, due to the bi-material effect (section 1.5.1), as well as frequency drift.
Ekinci et al. [50] used a similar expression to equation 11 to calculate the mass sensitivity (minimum detectable mass):

$$\delta m \approx \frac{1}{\Re} \left(\Delta f \frac{\omega_0}{Q} \right)^{1/2} 10^{(-DR/20)} \tag{12}$$

Where $\Re$ is the mass responsivity (equation 3), Δf is the measurement bandwidth and DR is the dynamic range (dB), expressed as:

$$DR = \log_{10}\left(\frac{k_B T}{m_{eff} \omega_0^2 \langle z^2 \rangle}\right) \tag{13}$$

1.6.2 Adsorption-desorption noise

Adsorption-desorption noise is caused by gas molecules randomly adsorbing on the surface of the resonator. The adsorption-desorption cycle is modeled with an adsorption rate $r_a = \frac{2}{5} \frac{p}{\sqrt{m k_B T}} s$ and desorption rate $r_d = v_d \exp\left(-\frac{E_b}{k_B T}\right)$ [50, 51], where p and T are the gas pressure and temperature, respectively. m is the mass of a gas molecule, s is the sticking coefficient ($0 < s < 1$), E_b is the binding energy between surface and atom, and ν_d is the desorption attempt rate. The effect this noise has on the mass sensitivity is expressed as follows (derivation is omitted):

$$\delta m \approx \frac{1}{2\pi} m \sigma_{occ} \left[N_a \arctan\left(2\pi \Delta f \tau_r\right) \right]^{1/2} \tag{14}$$

Where N_a is the number of sites for adsorption, σ_{occ} represents the variance in the occupation probability of a site ($\sigma_{\text{occ}}^2 = r_a r_d / \left(r_a + r_d\right)^2$) and τ_r is the correlation time for an adsorption-desorption cycle ($\tau_r = 1/(r_a + r_d)$).

1.6.3 Momentum exchange

Momentum exchanged between gas molecules and the resonator cause noise which behaves in a similar manner as thermomechanical noise [50]:

$$2 m_{\text{eff}} \left(\frac{k_B T}{E_c} \right)^{1/2} \left(\frac{\Delta f}{Q_{\text{gas}} \omega_0} \right)^{1/2} \tag{15}$$

Where Q_{gas} is the portion of the Q-factor due to gas dissipation (so without intrinsic damping), and is therefore a function of the pressure.

1.6.4 Transduction related noise

Besides the noise sources coming from the resonator itself and its environment, measuring and transducing the displacement into an actual signal also produces noise. In this subsection, three transduction related noise sources are discussed:

- Johnson-Nyquist Thermal Noise
- Shot noise
- Hooge (1/f) Noise

Since these noise sources are not dependent of the method of excitation, they will only briefly be discussed.

Johnson-Nyquist Thermal Noise

Originally observed by J.B. Johnson and later explained by Nyquist [52], Johnson-Nyquist thermal noise is caused by random thermally agitation of charge carriers in a conductor. It is the process which also drives the thermomechanical noise in equation 10. Its magnitude in terms of voltage or current is given by [53]:

$$\begin{aligned} V_{\text{th}} &= \sqrt{4k_B T R \text{BW}} \\ I_{\text{th}} &= \sqrt{\frac{4k_B T}{R} \text{BW}} \end{aligned} \tag{16}$$

It should be noted that T is the temperature of the resistor, not of the cantilever.

Shot noise

Shot noise is the result of the discrete nature of photons. If we look at photodiodes detecting a laser, the signal is not continuous. In fact, it can be seen as a succession of discontinuous pulses due to photons hitting the diode. Its magnitude scales with the square root of the average light intensity.

Hooge 1/f noise

Originating from fluctuations of the resistances of electrical components, 1/f noise owes its name because its magnitude increases as the frequency decreases. It's magnitude in terms of voltage and current was described by Hooge in his review on 1/f noise [54]:

$$\begin{aligned} V_{1/f} &= V_{\text{bias}} \sqrt{\frac{\gamma}{N_c} \ln\left(\frac{f_1}{f_0}\right)} \\ I_{1/f} &= \frac{V_{\text{bias}}}{R} \sqrt{\frac{\gamma}{N_c} \ln\left(\frac{f_1}{f_0}\right)}. \end{aligned} \tag{17}$$

Where V_{bias} is the voltage applied, γ is a proportionality constant which has to be empirically estimated, N_c is the number of carriers and f_0 and f_1 are the bandwidth frequencies. It should be noted that 1/f noise is temperature dependent since N_c is strongly dependent on temperature [27]. Other noise sources that contribute to $1/f$ noise in micro-mechanical resonators are fluctuations in magnetic material (when using magnetic excitation or sensing) [55], and gas adsorption-desorption [56].

1.7 Initial setup

The setup to be modified is an old AFM which was rebuilt by a previous master student, Ruben Guis [57]. Figure 9 shows a schematic view of the AFM, without the photothermal excitation mechanism. Figure 10 shows the initial design that enables this. It is connected to the left side of the schematic in figure 9, at the location of the eye.

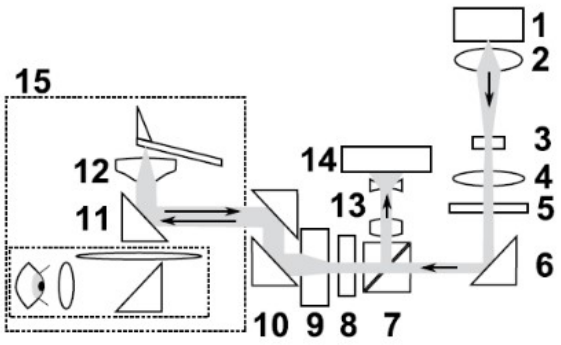

Figure 9: Schematic of the AFM without photothermal excitation [29]

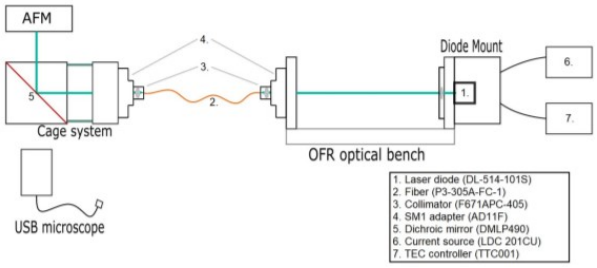

Figure 10: Schematic of the photothermal components [57]

The setup has a piezoelectric element built-in. Which means, that after appending the setup with the photothermal option, we have both excitation methods in one setup. This allows comparison without having to touch the cantilever or switch to a different setup. Driving the cantilever near its resonance is done using a phase-locked-loop.
The phase locked loop (figure 11) consists of a Voltage Controlled Oscillator (VCO), which is set to a certain frequency (usually close to the resonance of the cantilever). The signal is split into a reference signal and a drive signal. The drive signal passes through the cantilever, thus experiencing a phase shift. The phase of the reference signal is also shifted by a user defined amount. The difference between the phase shift after passing through the SMR and the user defined phase shift can now be determined by a phase comparator. In order to keep the frequency at our setpoint, the phase difference must remain zero. This is achieved by passing this difference through a loop gain (which is usually a PID controller) and back into the function generator.

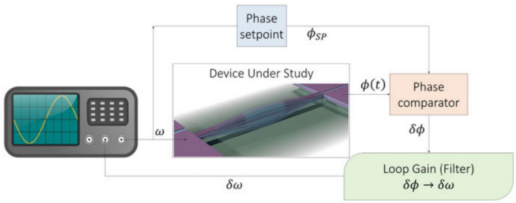

Figure 11: Schematic overview of a PLL [27]

1.8 Allan deviation

Cantilevers with a very high responsitivity can still be rendered useless if their frequency is very unstable. Frequency stability is often quantified using "Allan deviation". In short, Allan deviation uses the variance

of the change in frequency in a certain time interval. The Allan deviation is often plotted against different time intervals (gate times), which is an excellent method to quickly distinguish different noise types. For example, white noise varies a lot for short time intervals, but drift is usually only noticeable at large time intervals. Allan deviation is defined in the following manner [58, 59]:

$$\sigma_\nu^2(\tau) \approx \frac{1}{m} \sum_{k=1}^{m} \frac{(\bar{y}_{k+1} - \bar{y}_k)^2}{2} \tag{18}$$

Where $\bar{y}_k$ is the average frequency offset during the kth measurement interval (with interval length τ), and m is the total number of intervals. We can increase the number of intervals by using *overlapping Allan deviation*. Here, the start of one interval is not the end of the previous, but the intervals are overlapping (as seen in figure 12). This method improves confidence at the expense of higher computational time [60].

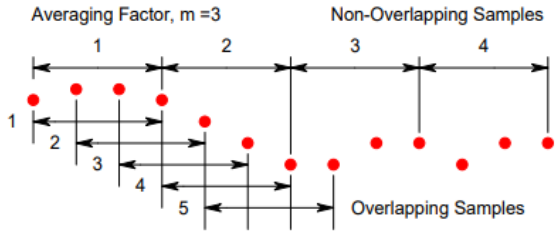

Figure 12: Overlapping samples [60]

By varying τ, we gain insight in the frequency stability on different timescales and the different noise sources present.
In mass measurement, a mass change Δm is linked to a resonance frequency shift Δf_n. The size of this frequency shift must be significant compared to the frequency imprecision, which is linked to Allan deviation. Therefore, a low Allan deviation is of great importance.

1.9 Research question(s)

Because the experimental setup allows for both piezo and photothermal excitation, the research questions are mainly aimed at the difference in results between these two. In AFM, the main argument for photothermal excitation is getting rid of spurious resonances, therefore the main research question is:

How do spurious resonances[1] *in microfluidic cantilevers change when changing from piezoelectric to photothermal excitation?*

Besides the potential decrease of spurious resonances, we are also interested in how the overall frequency stability changes. Using Allan deviation to quantify this gives us a good overview of the different noise processes and their influence:

How does the Allan Deviation change in microfluidic cantilevers when changing from piezoelectric to photothermal excitation?

2 Methods

This section describes the process of building the photothermal addition. While building the setup, a few complications arose which caused significant time delay in the project. Some of these complications will

[1] A spurious resonance is defined here as: A peak in the frequency response of the resonator significantly higher than the average amplitude value which is not a resonator mode

be touched upon in this section. While these problems are in hindsight not very complicated, they will be useful to discuss for anyone looking for more insight into the setup. The section is split in the following parts:

(A) **Enabling photothermal actuation:** Briefly describes the setup;

(B) **Fiber launching:** Redirecting the light into an optical fiber initially didn't work;

(C) **Blue laser reflections:** A lot of blue reflections appeared on the digital microscope which makes aligning difficult;

(D) **Insufficient degrees of freedom:** There were not enough degrees of freedom to align both the measurements and actuation laser;

(E) **Spot size:** The spot size of the blue laser is too large. This decreases the amount of energy absorbed by the cantilever;

(F) **Repeatability:** Some parts of the setup are badly soldered and not properly shielded from electromagnetic interference, causing repeatability issues;

(G) **Temperature fluctuations:** The laser diode temperature fluctuated too much, which caused strange artifacts in the measurements.

(H) **Laser controller frequency range:** The laser controller was only rated for DC-200Hz, so it had to be replaced.

2.1 Enabling photothermal actuation

Figure 9 shows the AFM setup, actuated by a piezo element in the cantilever holder. To enable photothermal actuation, we must direct an additional laser onto the cantilever. To allow for precise alignment, the laser position must be adjustable with a high resolution. On top of this, a camera is needed to monitor the laser spot on the cantilever. The exact location of the laser spot on the cantilever is important, as discussed in the introduction. The final setup is shown in figure 13. The laser is a 405nm 40mW diode, which is coupled into a multi-mode optical fiber using a Fiberport collimator combination. The optical fiber is placed in a three degree-of-freedom rotation mount, which is then mounted on a two degree-of-freedom linear motion stage, to facilitate high resolution alignment in five degrees of freedom. The outgoing beam is collimated and passes a 50/50 beamsplitter (half of the beam is dumped), after which it enters the AFM via a 45° mirror. The blue laser goes through a 45° short wave pass 750nm dichroic mirror and a final objective (20mm EFL, NA 0.56, precision machined) before hitting the top side of the cantilever. The reflected beam then follows the same path back until hitting the 50/50 beamsplitter, where half of the beam is directed into a digital microscope.

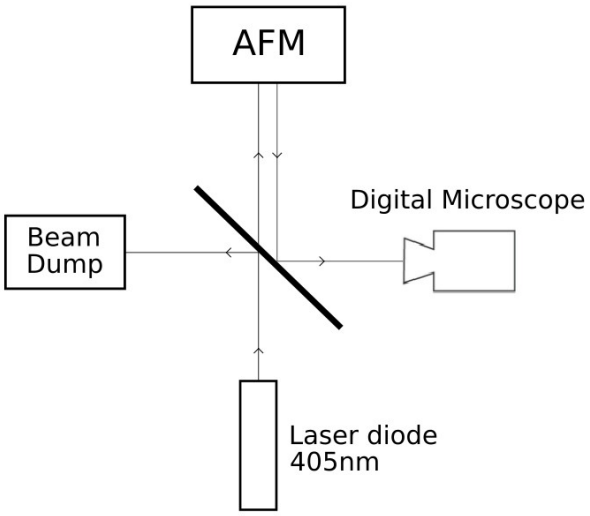

Figure 13: Final design

2.2 Fiber launching

One of the first steps in building this setup involves launching the blue laser into the optical fiber. Initially, a single-mode optical fiber was ordered. The alignment of a single-mode fiber is generally more difficult compared to multi-mode fibers because of the small core diameter. Launching the laser into the single-mode fiber with our available hardware was more difficult than initially thought. Switching to a multi-mode fiber solved this problem, sufficient launching was achieved shortly afterwards. Later on in the project, the negative effects of a larger core diameter on the eventual spot size were found. This issue will be explained later this section.

2.3 Blue laser reflections

When trying to align the laser in this configuration, strange reflections show up (figure 14). Initially, the Anti-Reflection Coating (ARC) of the AFM objective was thought to be the problem. Since the ARC was not designed for the wavelength of the blue laser. The blue laser could reflect in between the coating material and the lens material. This would explain the multiple reflections decreasing in intensity as seen in figure 14. To further investigate this theory, the same lens without an ARC was placed in the AFM using a 3D printed mounting bracket. Unfortunately, the reflections remained present.
After a thorough trial and error process, we found the ARC of the dichroic mirror shown in figure 10 to be the problem. It is likely that the reflections only account for a small percentage of the intensity, and should in theory not pose a problem for actuation. They do however pollute the image captured by the digital microscope, making alignment harder than it already is. Besides this, the dichroic mirror also blocks reflected light from the cantilever for 98.9% from hitting the microscope, severely weakening the most important spot on the image.

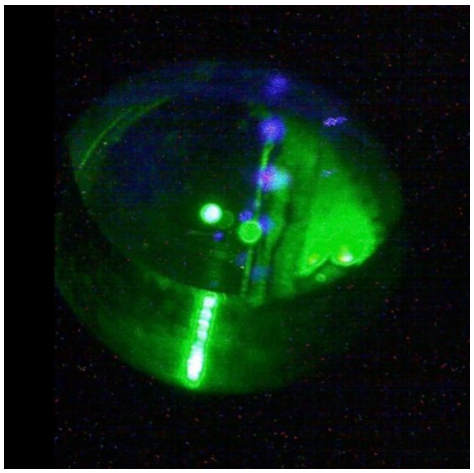

Figure 14: Reflections of the blue laser captured by the digital microscope

For the two reason stated above, the dichroic mirror was replaced by a 50/50 beamsplitter (Thorlabs EBS01 1") which was the most suitable beamsplitter in lab storage. An 8:92 (R:T) briefly replaced the 50:50 beamsplitter, but only a very limited amount of light reflected back onto the optical microscope. This made aligning very difficult. To overcome this issue, the 50:50 beamsplitter was placed on a 90° flip mount. When the alignment is done, the beamsplitter is no longer needed and thus it can be flipped away from the path of the laser. Now, 100% of the laser light passes onto the cantilever.

2.4 Insufficient degrees of freedom

The alignment screws on the AFM move the objective in X, Y and Z direction. The Z direction can be used to alter the focus of the spot onto the beam. Since using these screws is the only method to align the red laser, the blue laser must be aligned independently. The initial designs already houses three degrees of freedom using the tilt-plate. However, the only way to translate the blue laser in X and Z direction is by manually unscrewing and moving the pole. This method of translation is too coarse, and must be upgraded. The setup was therefore enriched by adding two manual linear stages, connected with a 90° corner. This enabled very fine translation of the blue laser, on top of the already present fine rotation.

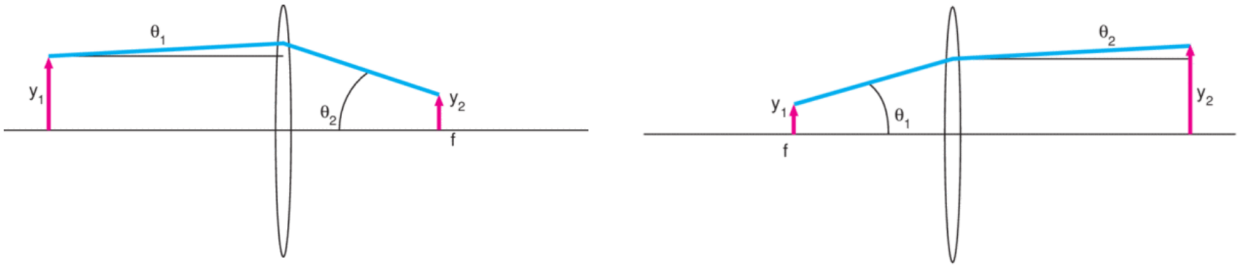

(a) (b)

Figure 15: (a) The divergence angle of a beam (θ_1) is related to the final spot size (y_2) [61], (b) The size of the light source (y_1) is related to the divergence angle (θ_2) [61]

2.5 Spot size

A small laser spot size is important. If a spot hitting the cantilever is too large, parts of it will "spill" over the edge, leading to a lower effective intensity. In case of the red laser, this will cause the signal strength to drop and thus the signal to noise ratio to rise. For the blue laser, a lower effective intensity means a lower actuation amplitude (also contributing to a decrease in signal to noise ratio) Both the red and the blue laser pass through the same objective, focusing the respective beams onto the cantilever.
One problem we encountered while aligning, was the blue spot size being too large, leading to no actuation because of a low effective intensity. This large spot size is due to two effects:

- Focal shift;
- Poor collimation

A big contributor to this problem was focal shift (a slightly different focal length due to a different wavelength). In our case, the theoretical focal shift was 0.664mm, leading to a increase in spot size of roughly 0.2mm (focal shift calculation is shown in appendix A). One method to minimize this effect is to slightly alter the focus to spread this difference out over the two laser spots (slightly increasing the red spot size, while decreasing the blue spot size). A more ideal case would be to replace the lens with one having a smaller focal shift. This focal shift will be considered in selecting a more optimal lens in the next subsection.
A second, more influential effect is a poor divergence angle. The divergence angle of a beam passing through a convergent lens will affect the spot size after focus (figure 15a).

$$y_2 = \theta_1 \cdot f \tag{19}$$

Where y_2 is the spot radius, θ_1 the divergence angle and f the focal length of the lens. The reason that the divergence angle is poor, is partly due to combining a collimator designed for single-mode fibers with a multi-mode fiber. But mostly due to the large core size of the multi-mode fiber (200μm), compared to the core size of a single-mode fiber (2.4μm). Changing to a single-mode fiber would decrease the divergence angle and spot size radius (equation 20 and 19 respectively) by at least a factor 100. Figure 15b shows a schematic of this effect, which follows the following equation:

$$\theta_2 = y_1 \cdot f \tag{20}$$

Now, θ_2 is the divergence angle and y_1 is the light source radius (in accordance to figure 15b). The divergence angle is between 1.5° and 2°, which means a spot size of around 1mm. Figure 20 clearly shows the size difference between the two laser spots.
Another way to improve the spot size is by using a different lens. Namely, a lens with a more favourable focal shift. When selecting an optimal lens for this setup, the following aspects need to be considered:

- **Focal length:** The focal length should be somewhere between 15-20mm. This is because of the AFM design: the range-of-motion of the focusing degree-of-freedom is limited
- **Anti Reflectance Coating (ARC):** The ARC of the lens must cover both the wavelength of the blue laser (405nm) as well as the wavelength of the red laser (785nm)
- **Focal shift:** Due to chromatic aberrations, a lens has a slightly different focal length for different wavelengths (focal shift). If this focal shift becomes too large, it becomes impossible to properly focus both lasers at the cantilever.
- **Lens diameter:** Of course, the lens should fit in the AFM, which means the diameter should not exceed 25mm. However, when needed, a lens can be smaller. The downside of a smaller lens is a

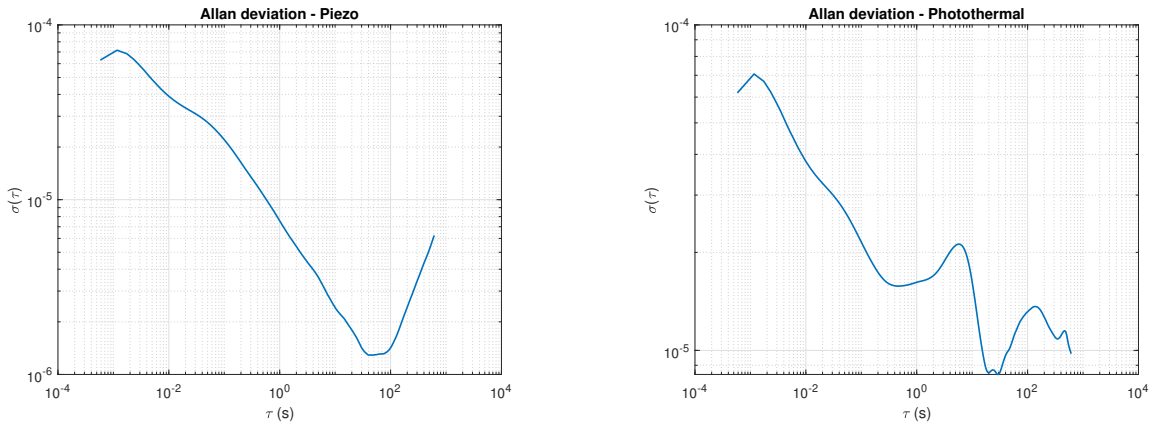

(a) (b)

Figure 16: (a) Frequency stability of piezo actuated AFM cantilever (b) Frequency stability of photothermally actuated AFM cantilever

decrease in optical leverage, which is linearly proportional to the signal-to-noise ratio [29] (figure 17):

$$\frac{ds}{dz} = \frac{2F}{L}\left(1 + \tan^2(\theta)\right), \theta = \arctan\left(\frac{s}{F}\right) - 2\alpha_1 \tag{21}$$

$$SNR \propto \frac{ds}{dz} \tag{22}$$

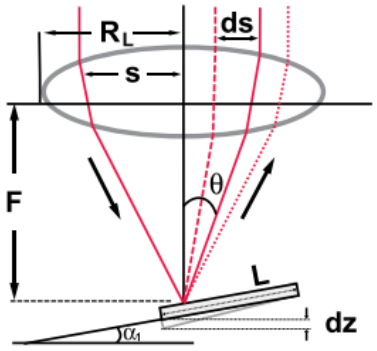

Figure 17: Optical leverage [29]

Taking all these points into account, Thorlabs 0.5" achromatic doublet: "AC127-019-AB" seems like the best candidate. The AR coating covers both wavelengths, the focal length is within bounds and the focal shift is very minimal (80 μm). The only downside is the smaller diameter, which will decrease the SNR with about 24% according to equation 21.

2.6 Repeatability

A fair comparison between any two measurements is impossible when the experimental setup shows poor repeatability. Important aspects of repeatability are: constant environment (temperature, pressure, humidity), constant setup configuration (placement of optical components, controller settings, laser current

settings), constant noise sources (proper electromagnetic shielding from neighbouring devices). One weakness in our setup regarding repeatability is a homemade cable between the photodiodes and the summing module [57] which is unshielded, and has open connections. Additionally, the solder is weak and breaks often when touched. A custom Printed Circuit Board (PCB), together with a metal box to minimize electromagnetic interference was designed and purchased to overcome this. These parts are however not functional yet.

2.7 Temperature fluctuations

During the first measurements, strange artifacts showed up in the Allan deviation plot when actuating photothermally (figure 16b, between $\tau = 1s$ and $\tau = 20s$). It turns out that these artifacts are due to a periodicity in the time signal (time signal is shown in appendix B). The periodicity is caused by temperature fluctuations: The laser diodes are temperature controlled by a PID controller and this controller is unable to properly control the temperature instabilities. The intensity output of the laser is temperature dependent (inversely). This means that changes of the laser diode temperature ultimately result in changes in temperature of the cantilever, which then slightly changes its resonance frequency. This causes the periodicity which the PID controller is unable to counteract - and instead keeps it going. This can be shown by comparing Allan deviation measurements with and without the temperature controller turned on (figure 18).
The solution to the resonance frequency fluctuations is a lower drive current. The lower drive current causes the laser intensity to drop, thus producing less heat. This makes it easier for the PID controller to stabilize.

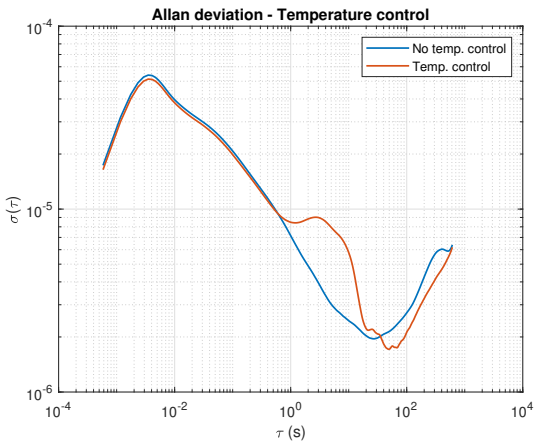

Figure 18: Frequency stability of photothermally actuated AFM cantilever with and without temperature control

2.8 Laser controller frequency range:

The initial laser diode controller (Thorlabs LDC201C) is only rated for up to 200Hz. Above 200Hz, the peak to peak current which is send to the laser will decrease with increasing frequency. Smaller cantilevers and higher modes are therefore especially difficult to excite with this controller because of their relatively high frequency.
To solve this, the controller was replaced with a similar version rated for DC-150kHz (Thorlabs LDC205C). Although the output current of this controller also decreases with increasing frequency, the rate at which this happens is much smaller. This decrease in current was measured for both controllers and is plotted in appendix C.

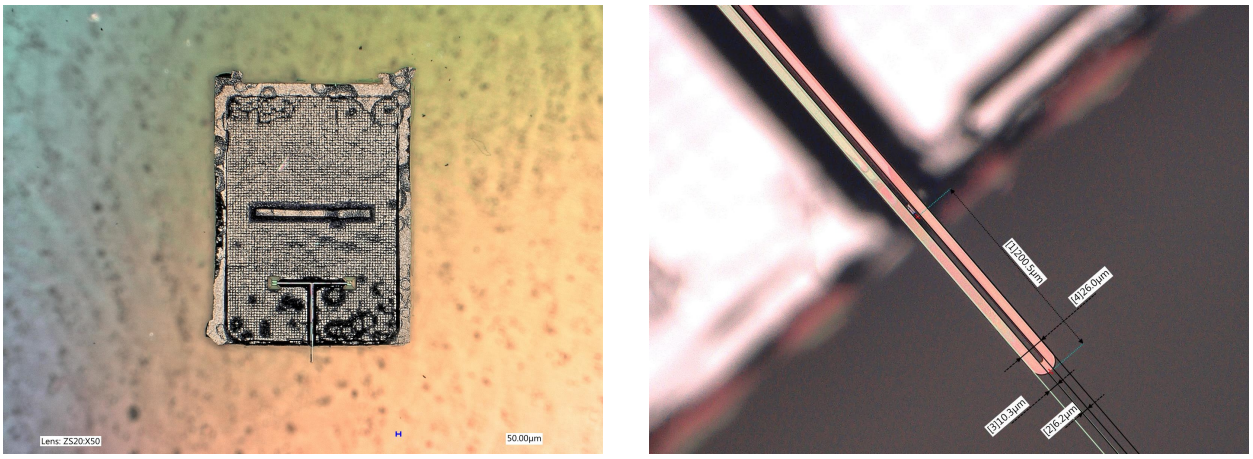

(a) (b)

Figure 19: Microfluidic cantilever (a) top view and (b) closeup with dimensions

2.9 Overview of the final setup

After several stages of improvement, the final setup is shown in figure 13. The laser light is launched into a multi-mode fiber and then collimated into free space. The laser then passes through the 50/50 beamsplitter while aligning. After alignment is optimized, the beamsplitter is flipped away from the laser path. The laser can be accurately positioned using the 2 DoF motion stage and the 3 DoF rotational mount. The blue laser light that reflects off the cantilever (while aligning) is reflected on the 50/50 beamsplitter onto the optical microscope.

2.10 Microfluidic cantilevers

The next step, after the AFM cantilevers, is microfluidic cantilevers. Images taken with an optical microscope of the cantilever are shown in figure 19, along with their rough dimensions. Usually, these cantilevers are glued to microfluidic channels which are connected to a syringe pump to facilitate flow. However, these microfluidics are not necessary for determining frequency stability and study spurious peaks. Besides this, they increase the chance of failure. Previous master students have reported frequent failures of the microfluidic connections [49]. Therefore, these connections will be omitted and the cantilever will be manually filled.

Ideally, to prevent evaporation, the cantilever should be capillary-filled with a high vapour pressure fluid. However, experiments with diethyl carbonate were unsuccessful because the relatively high surface tension prevents the fluid from entering the channel. Further experiments with water-glycerol solutions showed more promise. This is because, before filling, the cantilever is made hydrophilic by exposing it to plasma. The area surrounding the reservoirs is therefore more hydrophilic compared to the inside of the channel, which drives the liquid inside. Due to time constraints, the filled cantilevers were never mounted inside the AFM for testing.

Because the cantilever is made of silicon dioxide, which has a reflectivity of approximately 3% [62], the cantilever is coated with a thin layer of gold (20-40nm). Without the gold coating, the red laser for detecting would hardly be reflected resulting in a very low signal. Additionally, the gold coating significantly amplifies the driving force due to the difference in thermal expansion (as described in equation 6).

Unfortunately, the spot size is much larger compared to the dimensions of the microfluidic cantilever. In theory, the spot size diameter is about 30 times too large (1mm compared to the 30μm width of the cantilever). Because of this only a small portion of the laser light is heating the cantilever. On top of this,

the resonance frequency of these cantilevers is almost 7 times higher compared to the AFM cantilevers, leading to a laser current decrease due to the laser controller. Because of these two factors, the measured deflections are much smaller than the AFM cantilever.

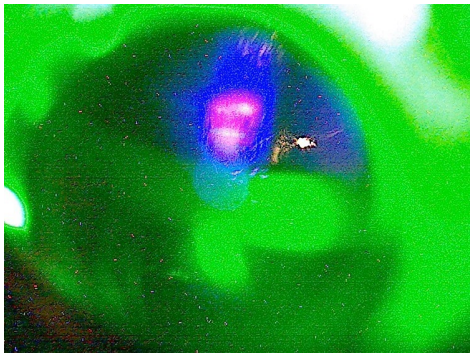

Figure 20: Difference in red and blue laser spot size

Frequency stability of a thermo-mechanical limited photothermal AFM

S.P. Paardekooper

***Abstract*—This paper describes the design of a photothermal addition on an existing Atomic Force Microscope (AFM) setup. It explores the differences between the more conventional, piezoacoustic method of actuation versus actuating photothermally in terms of frequency stability and spurious peaks. Measurements show that the frequency stability is limited by thermo-mechanical noise (for both piezoacoustic and photothermal actuation) and spurious peaks are completely resolved using photothermal actuation.**

I. Introduction

One of the most conventional methods to excite AFM cantilevers is by using a piezo-acoustic actuator. These actuators are usually placed on the chip holder, and vibrate the cantilever indirectly. Because of the indirect nature of this vibration, objects nearby will also vibrate. Their resonance peaks, along with the resonance peaks of the piezo itself, show up in the final frequency response. These "spurious peaks" are unwanted because they make it hard to find the cantilever resonance. One way to remove these peaks, is by changing the actuation method to photothermal actuation. Photothermal actuation uses a laser to locally heat the cantilever, which is usually coated with a thin metal film. The increase in temperature causes the cantilever to expand. Due to the difference in thermal expansion between the cantilever and the metal coating, the cantilever will bend. Modulating the intensity of this actuation laser will cause the cantilever to vibrate. Because this actuation method excites very locally, there are no spurious peaks.

Because (dynamic) AFMs and other resonance based sensing methods heavily rely on changes in resonance frequency, it is imperative that this frequency remains stable. This frequency stability can be quantified using "Allan deviation", which is defined as follows:

$$\sigma_\nu^2(\tau) \approx \frac{1}{m}\sum_{k=1}^{m}\frac{(\bar{y}_{k+1}-\bar{y}_k)^2}{2} \tag{1}$$

Where $\bar{y}_k$ is the average frequency offset during the kth measurement interval (with interval length τ), and m is the total number of intervals.

The goal of this paper is to study the changes in spurious peaks and Allan deviation when changing the actuating method from piezo-acoustic to photothermal.

II. Method

Figure 1a shows a schematic of the AFM which was originally designed and built by Katan [1], and recently rebuilt by Guis [2]. For a detailed description of this AFM, the reader is referred to their respective papers. To enable photothermal actuation, the parts shown in figure 1b were added. They consist of a blue 405nm, 40mW laser diode. The laser light goes through a 50/50 beamsplitter mounted on a flip mount, the remaining light is dumped. The reflections from the AFM are partly reflected by the beamsplitter into a digital microscope for alignment. The beamsplitter is removed from the laser path using the flip mount as soon as the blue laser is aligned and the digital microscope is no longer needed. The laser diode is mounted in a three degree-of-freedom rotational mount, which is mounted on a two degree-of-freedom linear motion stage.

The PLL measurements are done using a lock-in amplifier (Zurich Instruments) with the controller bandwidth tuned to 100Hz. PID values are determined according to research by Olcum et al. [3]. The cantilever is a Nanosensors PPP-CONTR-20, 450μm long, 50μm wide and 2μm thick sillicon cantilever with a 30nm aluminium coating driven by a 405nm, 40mW laser diode which is controlled by a diode controller (Thorlabs LDC205C). Measurement is done with a 785nm, 25mW laser diode, controlled with the a similar controller (Thorlabs LDC201CU) using the optical lever method. Both lasers are kept on constant temperature using two TEC controllers (Thorlabs TTC001). The measurement laser light reflects off of the cantilever onto an array of photodiodes, which can then be used to measure the deflection of the cantilever. The photodiodes are connected to a

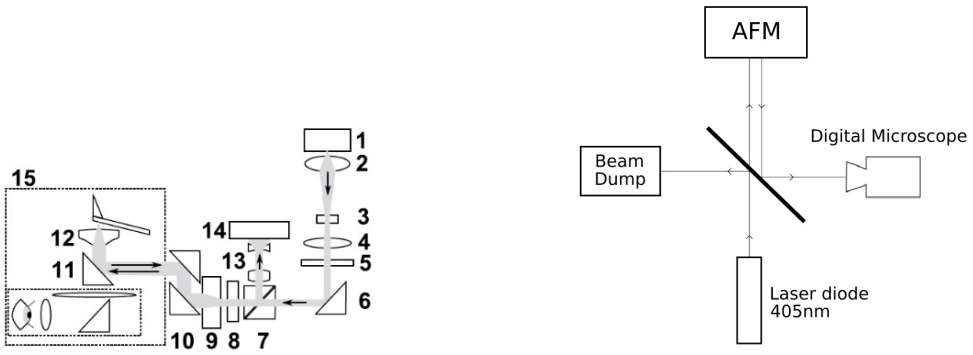

(a) (b)

Fig. 1: (a) Schematic of AFM setup (b) Schematic of photothermal addition

summing module, where they are individually gained and summed. Data analysis is done in Matlab. Both open-loop measurements (without PLL) and closed-loop measurements are performed. Open-loop measurements can be compared, and also transformed to pseudo closed-loop measurements by using the Matlab code by Manzaneque et al. [4]. Comparing open-loop results gives a better view of the differences since it doesn't include their respective control loops.

After validating the setup with rectangular AFM cantilevers, the switch to microfluidic cantilevers is made. These cantilevers are U-shaped, hollow and significantly smaller than the AFM cantilevers (200μm). Before testing these cantilevers, they are sputtered with a gold layer to improve their reflectivity (the reflectivity of SiO_2 is 3% [5], whereas gold has a reflectivity of 97% [6]).

III. Results

A. AFM Cantilever: Frequency stability

Measurements with the AFM cantilevers actuated with the piezo-element are shown in figure 2a (red line). These values are in agreement with literature, and show a minimum value of $\sigma_A = 4.48 \cdot 10^{-6}$ at $\tau = 129s$. The Allan deviation using the exact same setup, but now with photothermal actuation is shown in figure 2b (red line). The minimum value of $\sigma_A = 3.27 \cdot 10^{-6}$ here is slightly shifted right, and is at $\tau = 244s$. In the same figures, the pseudo closed-loop measurements (PCL) are also shown. These are open-loop measurements converted to closed-loop using an algorithm by Manzaneque et al. [4]. The PCL measurements show very good agreement with the actual CL measurements in both actuation cases. The shaded region in figures 2a and 2b represent the theoretical limit for our setup, which has been determined using the following formula [7]:

$$\sigma_{\mathrm{A}} \cong \frac{1}{2Q}\frac{\mathrm{N_T}}{S}\sqrt{\frac{1}{2\pi\tau}} \tag{2}$$

Where Q is the quality factor, S is the amplitude signal at resonance and τ is the gate time. N_T is the noise level at resonance, which was determined by the peak value of the spectral density around resonance. There is some uncertainty in determining the noise level, indicated by the upper and lower theoretical limit. As can be seen in the figure, the Allan deviation of both the piezo actuated and photothermally actuated cantilever are very close to this line. This suggests that the results are limited by the thermomechanical noise.

In addition to the first cantilever mode, the second mode has also been studied. The second mode is shown in figure 3, and shows up around 78kHz.

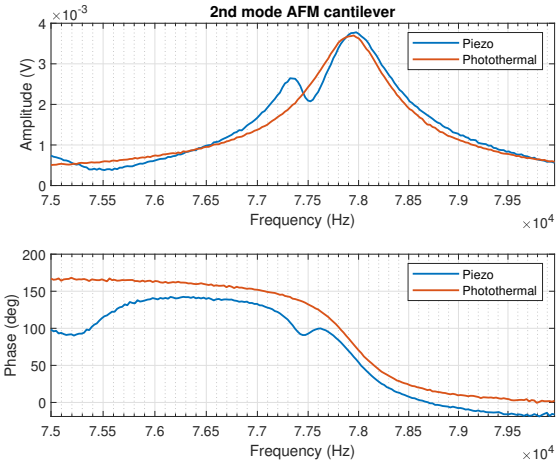

Fig. 3: 2nd AFM cantilever mode, actuated with both piezo and photothermal actuation

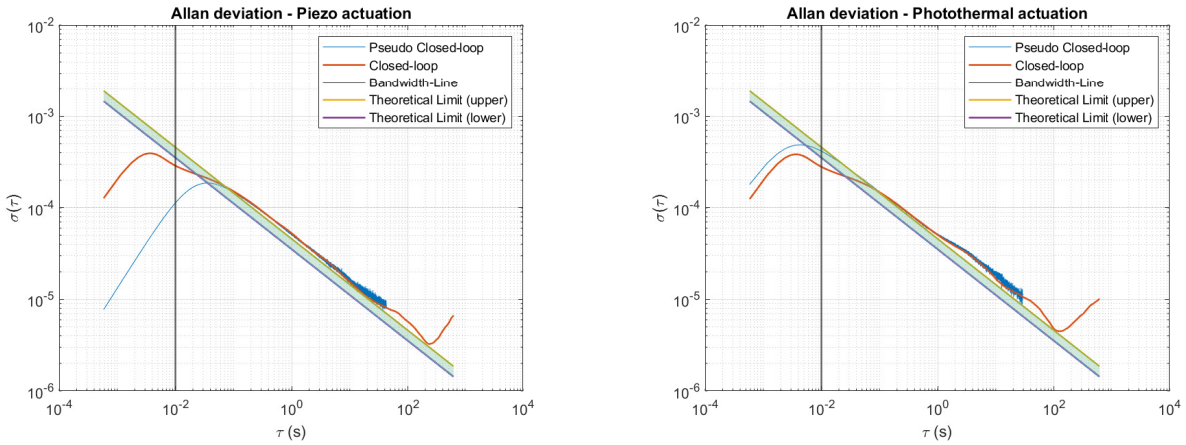

(a) (b)

Fig. 2: Allan deviation of (a) piezo-driven cantilever and (b) photothermally driven cantilever

There is a notable difference between the piezo and photothermal actuated resonance peak, namely the piezo shows a double peak. This could be due to a spurious peak, which is why the frequency stability was studied to see if there are any major differences. The Allan deviation plot of the second mode can be seen in figure 4.

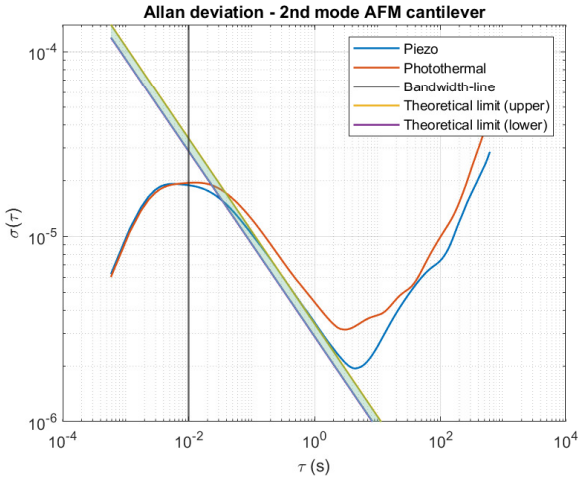

Fig. 4: Allan deviation of the 2nd AFM cantilever mode

The photothermal Allan deviation in this graph is higher because the amplitude during the measurement was slightly lower. Besides this, the photothermal line stops decreasing at around $\tau = 2s$, which is due to temperature fluctuations of the blue laser (similar to the first mode). Besides these two points, there are no notable differences. The minimum values are $\sigma = 1.9 \cdot 10^{-6}$ at $\tau = 4.4s$ for piezo actuation, and $\sigma = 3.1 \cdot 10^{-6}$ at $\tau = 3.0s$ for photothermal.

In this case, the difference in Allan deviation between the first and second mode is not very large. The Q-factor of this mode is much higher: 110, compared to 40 for the first mode, the signal is approximately twice as high in the first mode measurements compared to the second mode and the noise level is lower: $3.8\frac{\mu V}{\sqrt{Hz}}$, compared to $17\frac{\mu V}{\sqrt{Hz}}$ for the first mode. The significant difference in noise is due to the second mode having a higher effective stiffness. The equipartition theory states that, for each degree of freedom (each mode), cantilever movement z due to thermomechanical noise is given by:

$$\langle z^2 \rangle = \frac{k_B T}{k} \tag{3}$$

Where $\langle z^2 \rangle$ is the mean square displacement of the SMR, k_B is the Boltzmann constant, T temperature and k the effective stiffness of the cantilever. A higher effective stiffness leads to a lower deflection due to thermomechanical noise.

B. AFM Cantilever: Spurious peaks

Spurious peaks are found by sweeping from 10kHz to 350kHz. For piezo actuation, these results are shown in figure 5a. Above 70kHz, a lot of peaks show up, it is likely that these peaks are resonances of the piezo element or the cantilever holder. Figure 5b shows the same sweep for photothermal actuation. In contrast to piezo, no peaks are found besides the resonance frequency at 12.5kHz and the second mode at 78kHz.

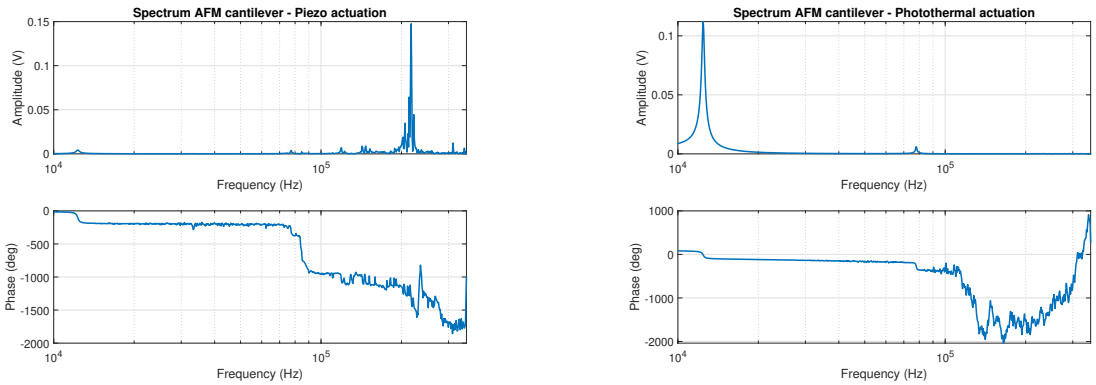

(a) (b)

Fig. 5: Sweep from 10kHz to 350kHz for both a (a) piezo actuated and (b) photothermally actuated AFM cantilever

C. Microfluidic cantilever: Spurious peaks

The presence of spurious peaks is also studied for the microfluidic cantilever. Again, a large frequency sweep (10kHz to 450kHz) is performed, which is shown in figure 7a for piezo actuation, and 7b for photothermal. Because these cantilevers are much smaller, a large portion of the blue laser light is lost due to it spilling over the edge. This caused the deflection, and thus the signal, to be weak for the photothermal case.
The presence of spurious peaks is not as significant for this cantilever in comparison to the AFM cantilever. The behaviour around resonance is less smooth for the piezo case however, this becomes more clear when looking at figure 6. The peak in the piezo case looks much sharper, and the phase shifts from 0° to approximately 300°, compared to the photothermal case where the phase shifts the usual 180°.

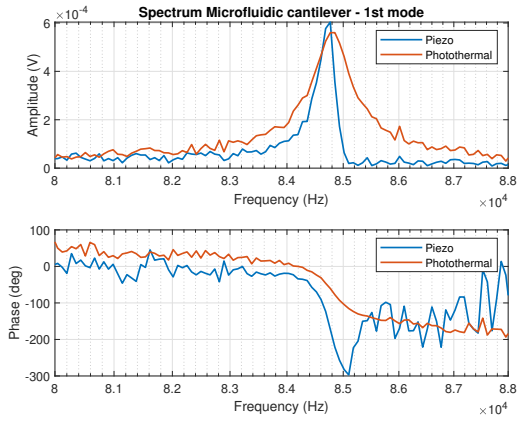

Fig. 6: First mode of a microfluidic cantilever

D. Microfluidic cantilever: Frequency stability

Frequency stability measurements of an empty microfluidic cantilever is shown in figure 8, both piezo and photothermally driven. As can be seen from the figure, the measured Allan deviation fits the theoretical limit very well for photothermal actuation. The minimum value is $\sigma = 6.9 \cdot 10^{-7}$ at $\tau = 46.9s$

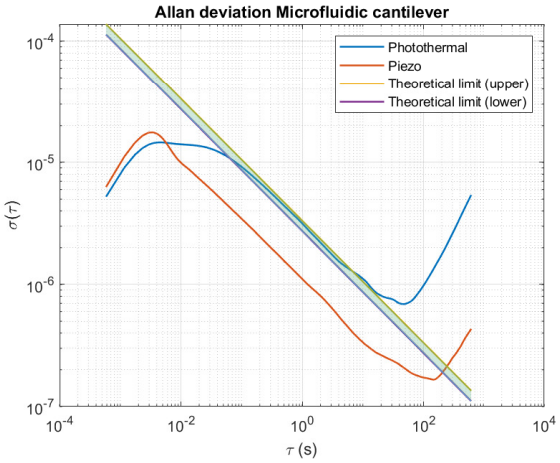

Fig. 8: Allan deviation of a photothermally driven (empty) microfluidic cantilever

Although the Allan deviation plot of the piezo has a similar shape, the values are much lower. The minimum value is $\sigma = 1.7 \cdot 10^{-7}$ at $\tau = 146.3s$. The reason these values are lower, is due to the spurious peak interfering with the first mode, as seen previously in figure 6. Because of this, the phase plot is much steeper around resonance, leading to a higher apparent Q-factor. This is also the reason why the values are

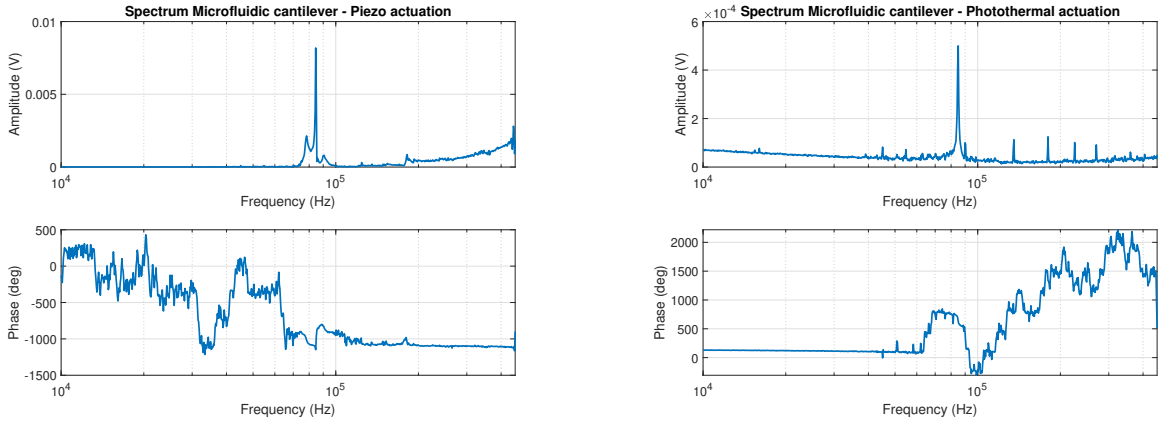

(a) (b)

Fig. 7: Sweep from 10kHz to 450kHz for both a (a) piezo actuated and (b) photothermally actuated Microfluidic cantilever

below the thermomechanical limit shown in the figure; a higher Q-factor means a lower theoretical limit for Allan deviation (equation 2).

IV. Discussion

The results of this study indicate that photothermal actuation and piezoacoustic actuation behave very similar in terms of frequency stability when there are no spurious peaks interfering with the resonance peak. There seem to be slightly more drift in the photothermal case, which is likely due to (blue) laser intensity variations at large timescales ($\tau > 100s$). In terms of spurious peaks however, the photothermal case shows huge improvements, with all peaks virtually removed. This result is consistent with literature, such as Tan et al. [8], who also studied the behaviour of spurious peaks with photothermal actuation.

V. Conclusion

In this paper, the design of a photothermal addition to an existing AFM was presented. This extra method of actuating allows for good comparison with the more conventional, piezoacoustic method. Results show comparable frequency stabilities with minimum Allan deviation values in the order of 10^{-6} for AFM cantilevers with a length of 500 μm, and 10^{-7} for the smaller (200μm) microfluidic cantilevers. Photothermal actuation shows more drift, which is likely due to temperature effects in the blue laser - but should be studied more thoroughly to be sure. In terms of spurious peaks: we see a significant improvement with photothermal actuation, removing all peaks except for the mode of interest, comparable to literature. The effect of this is clearly seen with the microfluidic cantilevers, where a spurious peak close the the fundamental mode causes a higher apparent Q-factor. In conclusion, photothermal is a promising method of actuation which shows great improvements over the more conventional piezo actuation.

References

[1] Allard Jules Katan. *Measuring interactions in fluids with small-cantilever AFM*. PhD thesis, 2007.

[2] Ruben Guis. Frequency stability in AFM. Technical report, 2020.

[3] Selim Olcum, Nathan Cermak, Steven C. Wasserman, and Scott R. Manalis. High-speed multiple-mode mass-sensing resolves dynamic nanoscale mass distributions. *Nature Communications*, 6:1–8, 2015.

[4] Tomas Manzaneque, Peter G. Steeneken, Farbod Alijani, and Murali K. Ghatkesar. Method to Determine the Closed-Loop Precision of Resonant Sensors from Open-Loop Measurements. *IEEE Sensors Journal*, 20(23):14262–14272, 2020.

[5] I. H. Malitson. Interspecimen Comparison of the Refractive Index of Fused Silica. *Journal of the Optical Society of America*, 55(10):1205, 1965.

[6] Dmitry I Yakubovsky, Aleksey V Arsenin, Yury V Stebunov, Dmitry YU Fedyanin, and Valentyn S Volkov. Optical constants and structural properties of thin gold films. *Optics Express*, 25(21):25574, 2017.

[7] Marc Sansa, Eric Sage, Elizabeth C. Bullard, Marc Gély, Thomas Alava, Eric Colinet, Akshay K. Naik, Luis Guillermo Villanueva, Laurent Duraffourg, Michael L. Roukes, Guillaume Jourdan, and Sébastien Hentz. Frequency fluctuations in silicon nanoresonators. *Nature Nanotechnology*, 11(6):552–558, 2016.

[8] Xinfeng Tan, Shuai Shi, Dan Guo, and Jianbin Luo. Dynamical characterization of micro cantilevers by different excitation methods in dynamic atomic force microscopy. *Review of Scientific Instruments*, 89(11):115109, 2018.

3 Overall conclusion

Frequency stability in resonance based sensing methods is extremely important. A major downside of the conventional piezoacoustic way of exciting resonators is a "forest-of-peaks" corrugating the frequency spectrum. Photothermal actuation is one way of solving this. In this thesis, a photothermal addition was built for a conventional AFM. Using this setup, the differences in frequency stability and frequency spectrum between the aforementioned actuation methods was studied. Findings show that, in terms of frequency stability, there aren't any large differences which will affect the performance of the application. Huge improvements were seen in terms of spurious peaks however, where all the unwanted peaks are resolved using photothermal actuation. This was the case for both conventional AFM cantilevers and microfluidic cantilevers. Limitations of the blue laser spot size in the setup made frequency stability analysis of microfluidic cantilevers impossible. In the next section, these limitations are addressed and recommendations are given on how to solve them. The now available method of photothermal actuation opens up a lot of interesting research, some example research questions are listed in the "Future work" section at the end of this thesis.

4 Recommendations

Towards the end of my thesis project, I've written down every improvement that I was not able to implement due to time constraints. I strongly recommend the next master student to take these recommendations into consideration.

- **Cantilever size is pushing the practical limits of the AFM:** When switching from the 500μm cantilevers to the 200μm, it became apparent that the current X and Y degrees of freedom on the AFM are relatively coarse. The smaller cantilevers in combination with some backlash in the mechanism makes aligning somewhat annoying. There are piezo's present on these DoF, but they are currently not working. Repairing these will most likely increase the alignment sensitivity.

- **Focal shift:** As mentioned earlier in this report: focal shift of the main AFM lens might limit the excitation of smaller cantilevers. Switching to the suggested lens will reduce this effect. Ideally one would use two separate lenses (one at the bottom of the AFM). However this will prevent mounting an AFM scanner in the future.

- **Collimation issues:** Collimation must be optimized in order to achieve small spot sizes. This means switching back to single-mode fibers. Replace the current collimator used to launch light from free space into the fiber for a lens (these collimators are not meant to launch laser light into a fiber). I would recommend trying to launch with the current alignment hardware - but chances are that a more accurate alignment stage needs to be installed.

- **Measurement laser defect:** There is a defect in the red laser fiber, causing it to vary in intensity when moved. This limits the repeatability of experiments. Replacing the laser-fiber combination should solve this problem.

- **Working space:** Currently, the setup is packed quite tightly on a small breadboard. I would recommend changing to a larger breadboard to allow for more room to experiment (placing extra lenses, beam-expanders etc.)

- **Better cantilever illumination:** Currently, only a small portion an LED light hits the cantilever. The poor illumination leads to more difficulty aligning. Installing a light source on a different location (e.g below the cantilever) will most likely increase the image quality and speed up the alignment process.

5 Future work

Besides improvements to the setup, there are plenty of interesting thesis subjects regarding this project. They will be listed in this section.

- **Investigate the actuation of higher modes for microfluidic cantilevers with photothermal actuation:** We've already seen higher modes of the AFM cantilever, but higher modes of the microfluidic cantilever is unfortunately not yet possible due to the large spot size. It would be interesting to see the differences in Allan deviance for these higher modes. Especially since the frequency of the higher modes tends to be much closer to spurious peaks. This will increase the chance to see a difference between actuating with a piezo vs. actuation photothermally. This will, in addition, open up the possibility to look into multi-mode measurements: Actuating and measuring with multiple modes simultaneously.
- **A thorough study on the temperature increase when actuating photothermally:** One of the biggest drawbacks on actuating microfluidic cantilevers photothermally is the extra heat introduced to the system. If temperatures surpass the boiling point of the liquid inside the cantilever, the measurement will likely fail, and perhaps even damage the microfluidic channel. A thorough FEM analysis is needed along with some experimental validation. Perhaps crossing the boiling point of the liquid under study can be detected visually using a microscope, or audibly by detecting bubble formation using a sensitive microphone. Or perhaps chemically by using some kind of temperature sensitive chemical reaction.
- **Mass measurements using photothermal actuation:** When the recommended improvements to the setup are executed, one can look into the mass detection limits of both actuation methods. This study will combine the open questions on temperature side-effects as well as on frequency stability. Answering those questions first is - in my opinion - the most sensible order.
- **Driving cantilever(s) to the onset of nonlinearity:** If the (improved) setup is capable of driving cantilevers to the nonlinear regime (with both piezo actuation as well as photothermally), a lot of interesting research topics open up. It could for example increase the mass sensitivity dramatically.

6 Self reflection

6.1 Planning

Figure 24 in appendix D shows the planning at the start of this project, approximately one year ago. Due to the practical nature of this project, this planning was very unsure. "Expanding AFM to enable photothermal excitation" took approximately 8 weeks longer to complete than initially thought, partly due to the complications discussed in this thesis. Because of this, my planning had to be adjusted halfway through this year. I decided to, in consultation with my supervisors, simplify the microfluidic part of my research. I would refrain from using complex microfluidics, and instead try to excite microfluidic cantilevers without any microfluidic connections. I was eventually able to excite empty microfluidic cantilevers photothermally, but measuring filled cantilevers was unfortunately not possible due to limited time.

6.2 Personal development

During the last year, I've seen myself grow both as a person and as a researcher. Due to the complexity of the project and my relatively little knowledge about optics, I was forced to step out of my comfort zone

and explore problems I initially knew little to nothing about. Despite this, I still managed to analyse and solve (most) problems that I have come across. This, in combination with feedback and reassurance from my supervisors has increased my self-esteem. I have noticed this improvement both in corresponding with my supervisors and others in the lab, as well as during my presentations.

Besides this, the clear division between the literature study and the thesis project has forced me to work more systematically. This is something I was initially not used to but quickly noticed it paying off. It was refreshing to notice that I frequently used the things I learned in my literature studies in practice. I will definitely continue working in a more systematic manner in the future.

There is still much to improve, especially in terms of planning. During my project, I was often distracted with experiments I found interesting. Even if they didn't fit into my scope or timeline. My supervisors often had to remind me to check and update my planning in order to graduate on time.

Lastly, the most obvious improvement: Practical knowledge. Working in a lab environment has taught me a lot. These are often things I would have never learned in a course. Especially in terms of optics, acoustics and signal processing. It has been a lot of fun learning in a practical environment like this.

References

[1] J Chaste, A Eichler, J Moser, G Ceballos, R Rurali, and A Bachtold. A nanomechanical mass sensor with yoctogram resolution. *Nature Nanotechnology*, 7(5):301–304, 2012.

[2] Nathan Cermak, Selim Olcum, Francisco Feijó Delgado, Steven C. Wasserman, Kristofor R. Payer, Mark A. Murakami, Scott M. Knudsen, Robert J. Kimmerling, Mark M. Stevens, Yuki Kikuchi, Arzu Sandikci, Masaaki Ogawa, Vincent Agache, François Baléras, David M. Weinstock, and Scott R. Manalis. High-throughput measurement of single-cell growth rates using serial microfluidic mass sensor arrays. *Nature Biotechnology*, 34(10):1052–1059, 2016.

[3] Mark M. Stevens, Cecile L. Maire, Nigel Chou, Mark A. Murakami, David S. Knoff, Yuki Kikuchi, Robert J. Kimmerling, Huiyun Liu, Samer Haidar, Nicholas L. Calistri, Nathan Cermak, Selim Olcum, Nicolas A. Cordero, Ahmed Idbaih, Patrick Y. Wen, David M. Weinstock, Keith L. Ligon, and Scott R. Manalis. Drug sensitivity of single cancer cells is predicted by changes in mass accumulation rate. *Nature Biotechnology*, 34(11):1161–1167, 2016.

[4] Arif E. Cetin, Mark M. Stevens, Nicholas L. Calistri, Mariateresa Fulciniti, Selim Olcum, Robert J. Kimmerling, Nikhil C. Munshi, and Scott R. Manalis. Determining therapeutic susceptibility in multiple myeloma by single-cell mass accumulation. *Nature Communications*, 8(1), 2017.

[5] Syed Asad Manzoor Bukhari, M. Faheem Khan, Ankur Goswami, Ryan McGee, and Thomas Thundat. Thermomechanical analysis of picograms of polymers using a suspended microchannel cantilever. *RSC Advances*, 7(14):8415–8420, 2017.

[6] N Umeda. Scanning attractive force microscope using photothermal vibration. *Journal of Vacuum Science & Technology B: Microelectronics and Nanometer Structures*, 9(2):1318, 1991.

[7] Glenn C. Ratcliff, Dorothy A. Erie, and Richard Superfine. Photothermal modulation for oscillating mode atomic force microscopy in solution. *Applied Physics Letters*, 72(15):1911–1913, 1998.

[8] Stefan W Stahl, Elias M Puchner, and Hermann E Gaub. Photothermal cantilever actuation for fast single-molecule force spectroscopy. *Rev. Sci. Instrum*, 80:73702, 2009.

[9] Holger Adam, Sebastian Rode, Martin Schreiber, Kei Kobayashi, Hirofumi Yamada, and Angelika Kühnle. Photothermal excitation setup for a modified commercial atomic force microscope. *Review of Scientific Instruments*, 85(2):23703, 2014.

[10] Valerio Pini, Bruno Tiribilli, Cecilia Maria Cristina Gambi, and Massimo Vassalli. Dynamical characterization of vibrating AFM cantilevers forced by photothermal excitation. *Physical Review B - Condensed Matter and Materials Physics*, 2010.

[11] Aleksander Labuda, Kei Kobayashi, Yoichi Miyahara, and Peter Grütter. Retrofitting an atomic force microscope with photothermal excitation for a clean cantilever response in low Q environments. *Review of Scientific Instruments*, 83(5):53703, 2012.

[12] Michel Godin, Andrea K Bryan, Thomas P Burg, Ken Babcock, and Scott R Manalis. Measuring the mass, density, and size of particles and cells using a suspended microchannel resonator. *Applied Physics Letters*, 91(12):123121, 2007.

[13] Thomas Braun, Viola Barwich, Murali Krishna Ghatkesar, Adriaan H Bredekamp, Christoph Gerber, Martin Hegner, and Hans Peter Lang. Micromechanical mass sensors for biomolecular detection in a physiological environment. *Physical Review*, page 9, 2005.

[14] I. Lee, K. Park, and J. Lee. Note: Precision viscosity measurement using suspended microchannel resonators. *Review of Scientific Instruments*, 83(11), 2012.

[15] Stefan Weigert, Markus Dreier, and Martin Hegner. Frequency shifts of cantilevers vibrating in various media. *Applied Physics Letters*, 69(19):2834–2836, 1996.

[16] Bram van den Brink, Farbod Alijani, and Murali Krishna Ghatkesar. Experimental setup for dynamic analysis of microand nano-mechanical systems in vacuum, gas, and liquid. *Micromachines*, 10(3), 2019.

[17] Thomas Braun, Murali Krishna Ghatkesar, Natalija Backmann, Wilfried Grange, Pascale Boulanger, Lucienne Letellier, Hans Peter Lang, Alex Bietsch, Christoph Gerber, and Martin Hegner. Quantitative time-resolved measurement of membrane protein-ligand interactions using microcantilever array sensors. *Nature Nanotechnology*, 4(3):179–185, 2009.

[18] J Lee, R Chunara, W Shen, K Payer, K Babcock, T P Burg, and S R Manalis. Suspended microchannel resonators with piezoresistive sensors. *Lab on a Chip*, 11(4):645–651, 2011.

[19] Josephine Shaw Bagnall, Sangwon Byun, Shahinoor Begum, David T. Miyamoto, Vivian C. Hecht, Shyamala Maheswaran, Shannon L. Stott, Mehmet Toner, Richard O. Hynes, and Scott R. Manalis. Deformability of Tumor Cells versus Blood Cells. *Scientific Reports*, 5(December):1–11, 2015.

[20] Sangwon Byun, Sungmin Son, Dario Amodei, Nathan Cermak, Josephine Shaw, Joon Ho Kang, Vivian C Hecht, Monte M Winslow, Tyler Jacks, Parag Mallick, and Scott R Manalis. Characterizing deformability and surface friction of cancer cells. *Proceedings of the National Academy of Sciences of the United States of America*, 110(19):7580–7585, 2013.

[21] Thomas P Burg, Michel Godin, Scott M Knudsen, Wenjiang Shen, Greg Carlson, John S Foster, Ken Babcock, and Scott R Manalis. Weighing of biomolecules, single cells and single nanoparticles in fluid. *Nature*, 446(7139):1066–1069, 2007.

[22] P. Belardinelli, M. K. Ghatkesar, U. Staufer, and F. Alijani. Linear and non-linear vibrations of fluid-filled hollow microcantilevers interacting with small particles. *International Journal of Non-Linear Mechanics*, 93:30–40, 7 2017.

[23] K L Ekinci and M L Roukes. Nanoelectromechanical systems. *Review of Scientific Instruments*, 76(6), 2005.

[24] Annalisa De Pastina and Luis Guillermo Villanueva. Suspended micro/nano channel resonators: A review. *Journal of Micromechanics and Microengineering*, 30(4), 2020.

[25] Marc Sansa, Eric Sage, Elizabeth C. Bullard, Marc Gély, Thomas Alava, Eric Colinet, Akshay K. Naik, Luis Guillermo Villanueva, Laurent Duraffourg, Michael L. Roukes, Guillaume Jourdan, and Sébastien Hentz. Frequency fluctuations in silicon nanoresonators. *Nature Nanotechnology*, 11(6):552–558, 2016.

[26] Laser Doppler vibrometer - Wikipedia.

[27] Silvan Schmid, Luis Guillermo Villanueva, and Michael Lee Roukes. *Fundamentals of nanomechanical resonators*. 2016.

[28] Bernard Ouma Alunda and Yong Joong Lee. Review: Cantilever-based sensors for high speed atomic force microscopy. *Sensors (Switzerland)*, 20(17):1–39, 2020.

[29] Allard Jules Katan. *Measuring interactions in fluids with small-cantilever AFM*. PhD thesis, 2007.

[30] Xin Xu and Arvind Raman. Comparative dynamics of magnetically, acoustically, and Brownian motion driven microcantilevers in liquids. *Journal of Applied Physics*, 102(3):34303, 2007.

[31] Ken Ichi Umeda, Noriaki Oyabu, Kei Kobayashi, Yoshiki Hirata, Kazumi Matsushige, and Hirofumi Yamada. High-resolution frequency-modulation atomic force microscopy in liquids using electrostatic excitation method. *Applied Physics Express*, 3(6), 2010.

[32] Thomas P Burg. *Suspended Microchannel Resonators for Biomolecular Detection*. PhD thesis, Massachusetts Institute of Technology, 2005.

[33] Yoichi Miyahara, Harrisonn Griffin, Antoine Roy-Gobeil, Ron Belyansky, Hadallia Bergeron, José Bustamante, and Peter Grutter. Optical excitation of atomic force microscopy cantilever for accurate spectroscopic measurements. *EPJ Techniques and Instrumentation*, 7(1), 2020.

[34] Aleksander Labuda, Yoichi Miyahara, Lynda Cockins, and Peter H. Grütter. Decoupling conservative and dissipative forces in frequency modulation atomic force microscopy. *Physical Review B - Condensed Matter and Materials Physics*, 2011.

[35] J. Kokavecz and A. Mechler. Investigation of fluid cell resonances in intermittent contact mode atomic force microscopy. *Applied Physics Letters*, 91(2), 2007.

[36] A Labuda, K Kobayashi, D Kiracofe, K Suzuki, P H Grütter, and H Yamada. Comparison of photothermal and piezoacoustic excitation methods for frequency and phase modulation atomic force microscopy in liquid environments. *AIP Advances*, 1(2):22136, 2011.

[37] Natsumi Inada, Hitoshi Asakawa, Taiki Kobayashi, and Takeshi Fukuma. Efficiency improvement in the cantilever photothermal excitation method using a photothermal conversion layer. *Beilstein Journal of Nanotechnology*, 7(1):409–417, 2016.

[38] Daniel Kiracofe, Kei Kobayashi, Aleksander Labuda, Arvind Raman, and Hirofumi Yamada. High efficiency laser photothermal excitation of microcantilever vibrations in air and liquids. *Review of Scientific Instruments*, 82(1):113903, 2011.

[39] D Ramos, J Tamayo, J Mertens, and M Calleja. Photothermal excitation of microcantilevers in liquids. *Journal of Applied Physics*, 99(12), 2006.

[40] Robert A Barton, B. Ilic, Scott S Verbridge, Benjamin R Cipriany, Jeevak M Parpia, and Harold G Craighead. Fabrication of a nanomechanical mass sensor containing a nanofluidic channel. *Nano Letters*, 10(6):2058–2063, 2010.

[41] Søren Dohn. *Cantilever Based Mass Sensing Alternative Readout and Operation Schemes*. PhD thesis, Technical University of Denmark, 2006.

[42] F. Shen, P. Lu, S. J. O'Shea, K. H. Lee, and T. Y. Ng. Thermal effects on coated resonant microcantilevers. *Sensors and Actuators, A: Physical*, 95(1):17–23, 2001.

[43] Johann Mertens, Eric Finot, Thomas Thundat, Arnaud Fabre, Marie Hélène Nadal, Vincent Eyraud, and Eric Bourillot. Effects of temperature and pressure on microcantilever resonance response. *Ultramicroscopy*, 97(1-4):119–126, 2003.

[44] Felipe Aguilar Sandoval, Mickael Geitner, Éric Bertin, and Ludovic Bellon. Resonance frequency shift of strongly heated micro-cantilevers. *Journal of Applied Physics*, 117(23):234503, 2015.

[45] M. Hipp H. Bielefeldt J. Colchero O. Marti, A. Ruf and J. Mlynek. Mechanical and thermal effects of laser irradiation on force microscope cantilevers. *Ultramicroscopy*, 42-44(PART 1):371–378, 1992.

[46] Benjamin A. Bircher, Luc Duempelmann, Hans P. Lang, Christoph Gerber, and Thomas Braun. Photothermal excitation of microcantilevers in liquid: Effect of the excitation laser position on temperature and vibrational amplitude. *Micro and Nano Letters*, 8(11):770–774, 2013.

[47] Alex Masolin, Pierre Olivier Bouchard, Roberto Martini, and Marc Bernacki. Thermo-mechanical and fracture properties in single-crystal silicon. *Journal of Materials Science*, 48(3):979–988, 2013.

[48] Hamed Sadeghian, Chung Kai Yang, Khashayar Babaei Gavan, Johannes F.L. Goosen, W. J.M. Van Emile Der Drift, Herre S.J. Van Der Zant, Andre Bossche, Paddy J. French, and Fred Van Keulen. Some considerations of effects-induced errors in resonant cantilevers with the laser deflection method. *Journal of Micromechanics and Microengineering*, 20(10), 2010.

[49] Xin Hu. Precision Error in Mass Measurements using Metal-coated Microchannel Resonators. Technical Report September, Delft University of Technology, 2019.

[50] K. L. Ekinci, Y. T. Yang, and M. L. Roukes. Ultimate limits to inertial mass sensing based upon nanoelectromechanical systems. *Journal of Applied Physics*, 95(5):2682–2689, 2004.

[51] A N Cleland and M L Roukes. Noise processes in nanomechanical resonators. *Journal of Applied Physics*, 92(5):2758–2769, 2002.

[52] H. Nyquist. Thermal agitation of electric charge in conductors. *Physical Review*, 1928.

[53] J. B. Johnson. Thermal agitation of electricity in conductors. *Physical Review*, 32(1):97–109, 1928.

[54] F.N. Hooge. 1/f Noise. *Physica B+ C*, 83:14–23, 1976.

[55] Phillip Durdaut, Enrico Rubiola, Jean Michel Friedt, Cai Müller, Benjamin Spetzler, Christine Kirchhof, Dirk Meyners, Eckhard Quandt, Franz Faupel, Jeffrey McCord, Reinhard Knöchel, and Michael Höft. Fundamental Noise Limits and Sensitivity of Piezoelectrically Driven Magnetoelastic Cantilevers. *Journal of Microelectromechanical Systems*, 29(5):1347–1361, 2020.

[56] Sang Jin Kim, Takahito Ono, and Masayoshi Esashi. Mass detection using capacitive resonant silicon resonator employing LC resonant circuit technique. *Review of Scientific Instruments*, 78(8):85103, 2007.

[57] Ruben Guis. Frequency stability in AFM. Technical report, 2020.

[58] James A. Barnes, Andrew R. Chi, Leonard S. Cutler, Daniel J. Healey, David B. Leeson, E. Thomas McGunigal, James A. Mullen, Warren L. Smith, Richard L. Sydnor, Robert F.C. Vessot, and Gernot M.R. Winkler. Characterization of Frequency Stability. *IEEE Transactions on Instrumentation and Measurement*, 1971.

[59] David W. Allan. Statistics of Atomic Frequency Standards. *Proceedings of the IEEE*, 54(2):221–230, 1966.

[60] W J Riley. Handbook of Frequency Stability Analysis. Technical report.

[61] Newport Corporation. Focusing and Collimating. *Technical Note: Optics*, pages 6–8, 2014.

[62] I. H. Malitson. Interspecimen Comparison of the Refractive Index of Fused Silica. *Journal of the Optical Society of America*, 55(10):1205, 1965.

A Focal Shift calculation

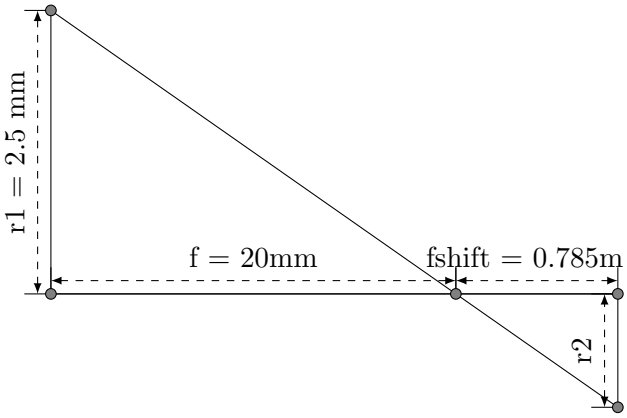

(a) Focal shift sketch

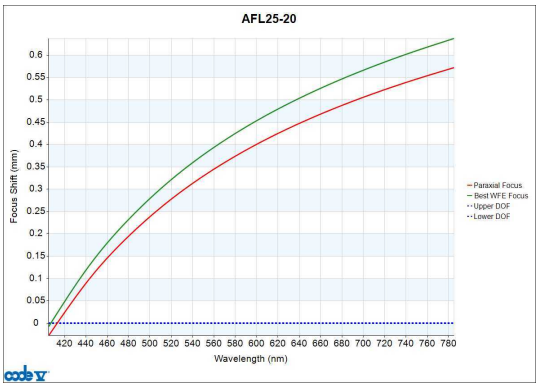

(b) Focal shift data (Thorlabs)

Figure 21

$$r_2 = f_{shift} \cdot \frac{r_1}{f}$$
$$r_2 = 0.664 \cdot \frac{2.5}{20} = 0.083mm$$
$$d_2 = r_2 \cdot 2 = 0.083 \cdot 2 \approx 0.17mm$$

B Resonant frequency vs time

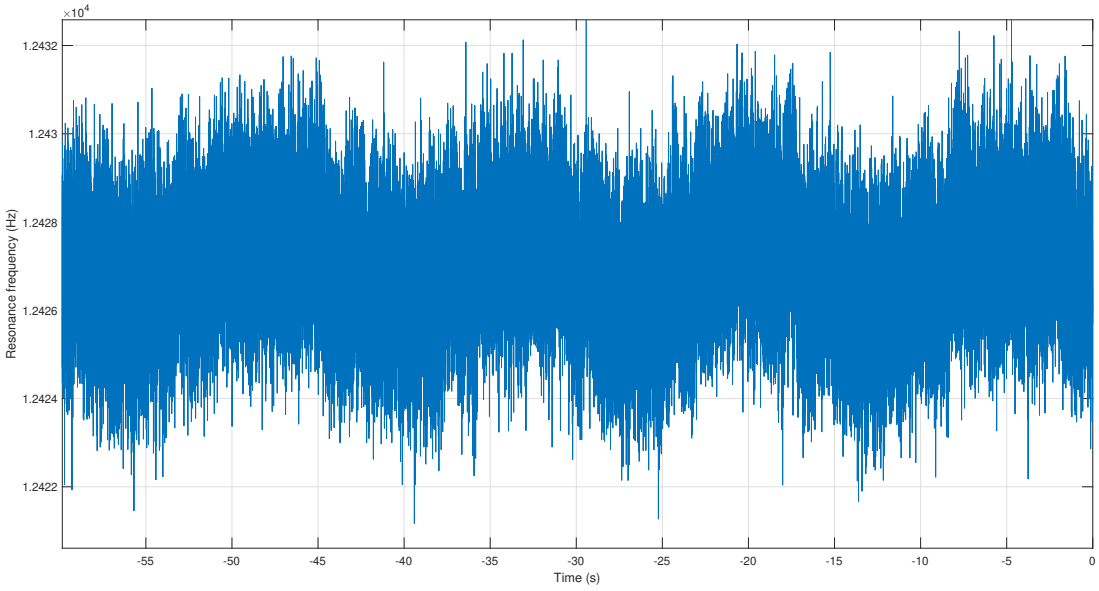

Figure 22: Small section of a 30 minute resonance frequency tracking measurement showing a clear periodicity

C Laser controllers frequency dependency

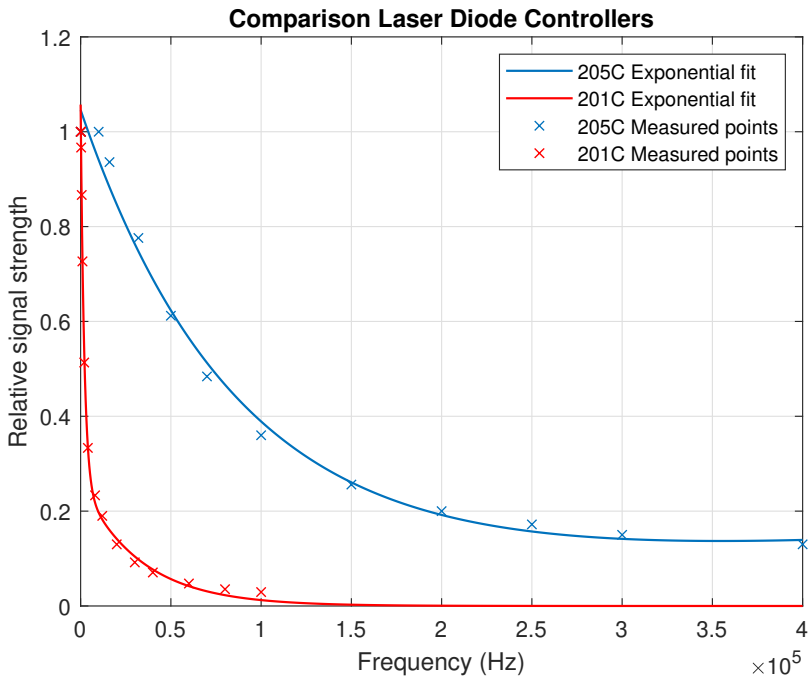

Figure 23: Relative output signal vs. frequency for both laser controllers

D Planning

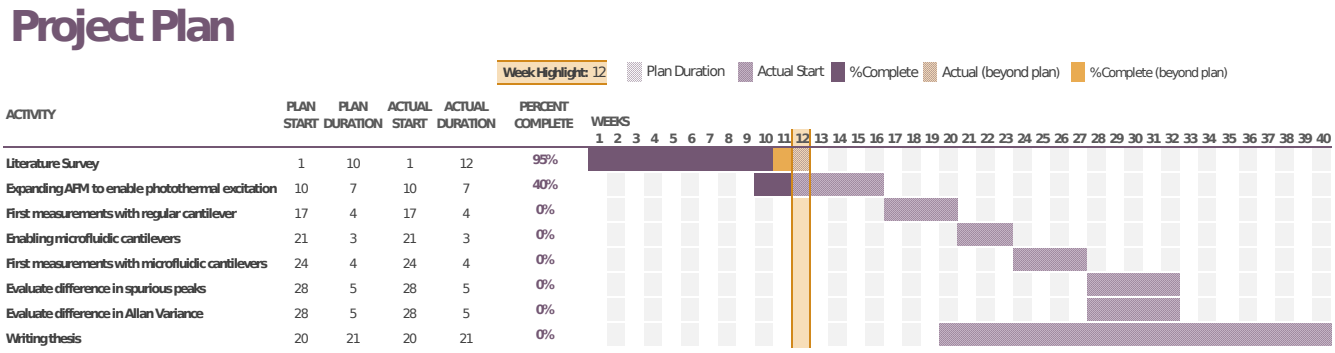

Figure 24: Planning at the start of this project